Tether-Inertial Localization for Drones on Mars

MSc Thesis Report

Dielof van Loon

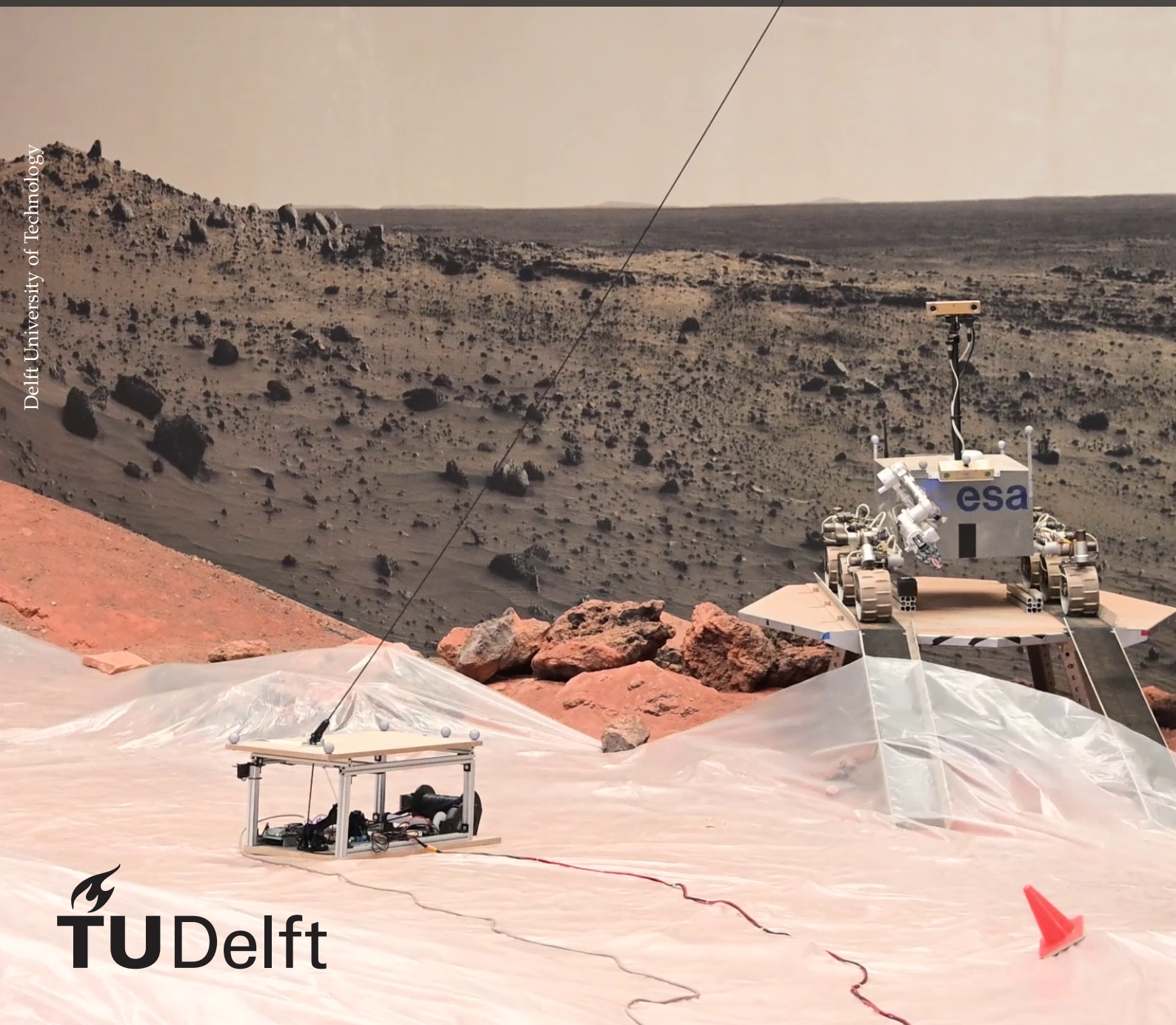

Delft University of Technology

TU Delft

[This page is intentionally left blank]

Tether-Inertial Localization for Drones on Mars

MSc Thesis Report

by

Dielof van Loon

to obtain the degree of Master of Science
at the Delft University of Technology,
to be defended publicly on Monday November 24th, 2025 at 13:00.

Thesis committee:	
Chair:	Dr. J.M. Prendergast
Daily Supervisors:	Ir. A. Bredenbeck
	Dr. L. Puck
Supervisor:	Dr. S. Hamaza
Place:	Faculty of Mechanical Engineering, Delft
Student number:	5346894
Project duration:	December, 2024 – November, 2025

Cover: Tethered Drone Experimentation in the Planetary Robotics Lab at ESA, ESTEC. ESA-SJM Photography (ESA Standard Licence).

An electronic version of this thesis is available at `http://repository.tudelft.nl/`.

TU Delft

[This page is intentionally left blank]

Preface

This thesis is the result of a valuable Masters period which not only taught me a lot about robotics, but also about me and my broad interests. I am grateful for the freedom I got while researching this topic as I dived into hardware, software, geometrics and algorithms.

I would like to thank my mentors, Anton, Lennart, Alex, Martin and Salua, for their advice and assistance. Also a thank you to my colleagues at ESA for the fun times and good conversations. Finally, my deepest thanks go to my family, friends, and Roos for providing both the support and distraction I needed along the way.

Dielof van Loon
Delft, November 2025

[This page is intentionally left blank]

Contents

[This page is intentionally left blank]

Part I

Introduction

[This page is intentionally left blank]

Introduction

Planetary exploration missions focused on resource extraction, habitability studies and the search of life require increasingly sophisticated autonomous robotic systems capable of reliable operation in harsh extraterrestrial conditions. Recent missions, such as NASA's Perserverance rover [1] and Ingenuity helicopter [2], have shown the potential and limitations of what is possible with modern technologies. Ingenuity demonstrated the viability of autonomous Unmanned Aerial Vehicles (UAVs) with their 72 successful missions before crashing into a sand dune [3]. This crash highlights several engineering challenges, created by the heavy constraints of extraterrestrial exploration, such as the unavailability of satellite-based positioning systems, susceptibility of vision-based navigation to failure in textureless environments such as sand dunes, and stringent Size, Weight, and Power (SWaP) budgets that restrict both computational resources and mission duration.

Tethering UAVs to ground-based rovers could present an architectural solution, enabling continuous power supply and high-bandwidth communication while transferring computationally intensive processing tasks to the base platform, thereby circumventing the drone's SWaP limitations. Several commercial Tether Management Systems (TMSs) are available and are used on Earth proving their viability in normal operation [4]. While providing a solution for payload and power capacity, the vulnerabilities in visual odometry algorithms highlighted above are still left to be solved.

This thesis investigates a fundamentally different approach to Tethered Unmanned Aerial Vehicle (TUAV) state estimation by treating the tether as a primary sensor, utilizing measurements of its length, tension, and angular orientation to compute the UAV's three-dimensional position relative to the base platform through a catenary equation that models a slack tether augmented with learned error correction.

Hence, this thesis aims to answer the following research question:

"How accurately can a tethered drone be localized relative to a rover using tether-based inertial sensing?"

The structure of this report is as follows. Part II presents the scientific article that addresses the above research question through experimental validation of the proposed Tether-Inertial Localization system. Part III provides a literature review examining the state-of-the-art in both conventional UAV localization methods and tether-based positioning approaches.

[This page is intentionally left blank]

Part II

Scientific Article

Tether-Inertial Localization for Drones on Mars

Dielof van Loon[1]

***Abstract*—Recent developments in planetary exploration have shown the potential of Unmanned Aerial Vehicles (UAVs), such as the Ingenuity helicopter that provided valuable mapping data. However, limited payload capabilities constrain the flight times and compute available for localization which restrict their applicability. By providing a tethered connection, issues such as battery and computational constraints are offloaded to the base rover. At the same time, the cable can be exploited for non-drifting localization. This work presents a novel Tether-Inertial Localization approach that uses tether length, and angle measurements to estimate the UAV pose relative to its base. The method combines a computationally efficient analytical catenary model with a Gaussian Process (GP) residual error compensation. This accounts for systematic sensor inaccuracies and model limitations under dynamic conditions. Experimental validation across circular, triangular, and figure-eight trajectories with tether lengths up to $4.5\,\mathrm{m}$ spanning 41 minutes of flight time with only the tether based estimate as position feedback, demonstrates estimation errors of $0.073\,\mathrm{m}$ average RMSE for the analytical model alone and $0.049\,\mathrm{m}$ average RMSE with GP enhancement. With this, we provide an alternative localization method to conventional vision or GNSS-based methods, providing similar accuracies for Tethered Unmanned Aerial Vehicles (TUAVs).**

***Index Terms*—Space Robotics and Automation; Aerial Systems: Perception and Autonomy; Localization**

Fig. 1. The Tether Management System with the HolyBro QAV250 drone next to the MaRTA rover in the Mars yard of the PRL at ESA, ESTEC. The drone uses the TI Localization system to compute its position based on the physical properties of the tether: tether length and angles.

I. Introduction

The growing focus on celestial body exploration for applications including resource extraction and habitability assessment has increased the need for autonomous planetary exploration systems. Current examples include the Perseverance rover [1] and the Ingenuity helicopter [2]. Aerial robots in planetary exploration can enhance the mission performance as distant objects are detected more reliably, radio beacons can extend further beyond the horizon and data can be collected from a stable drone platform. The Ingenuity helicopter proved the viability of aerial planetary robotics on Mars throughout its 72 missions, where it provided valuable mapping data; nevertheless, its final mission concluded in a crash caused by insufficient features for its vision-based localization system [3]. The Ingenuity experience demonstrates that UAVs continue to encounter substantial challenges, including restricted payload capabilities. These result in limited flight duration due to battery constraints and limited processing of on-board image feeds for localization due to processor weight and power constraints. One way to address these challenges is to incorporate a tether that links the UAV to a companion rover. The tether can provide continuous power, compute, and reliable communication links, thus extending flight duration and enabling more sophisticated computational tasks. While TUAV systems are commercially accessible [4], a significant gap remains: none of these systems utilize the physical properties of the tether—such as length and angles—as a source for localizing the attached UAV relative to the rover. In this work, we introduce a novel Tether-Inertial (TI) Localization approach using a catenary model and a GP. Our system incorporates length, angle, and tension sensors to measure all relevant tether state variables, enabling accurate estimation of the UAVs position relative to the rover. Thereby enabling robust position control even in feature-sparse environments. The contributions of this work are:

- The development of an analytical catenary model for computationally efficient estimation of the TUAV's position and its uncertainty.
- A Gaussian Process, trained from pairs of tether states and residual errors, to compensate the non-linear effects causing discrepancies between the analytical position estimate and the ground truth.
- The comprehensive experimental validation of the Tether-Inertial Localization approach using a custom built Tether Management System (TMS).

[1]Dept. of Cognitive Robotics, Faculty of Mechanical Engineering, TU Delft, The Netherlands

II. Related Work

Several approaches have been explored for localizing TUAVs in GNSS-denied environments. Focusing specifically on methods that exploit tether information, two main categories emerge: (i) approaches that assume the tether remains taut [5, 6], and (ii) approaches that explicitly account for the tether's flexible nature [7, 8, 9]. The work presented in [8] employs a commercial TMS that measures elevation and azimuth angles of the tether departure point. The tether angle at the drone is inferred from the drone's attitude relative to the horizontal plane. The position estimation uses a taut tether assumption with corrections for slacking tether effects. Indoor static validation with motion capture ground truth achieved $0.37\,\mathrm{m}$ average error at maximum tether lengths of $3.25\,\mathrm{m}$. Borgese et al. [9] use custom hardware mounted on a rover which measures angles at both ends of the tether, but uses a fixed length tether. The tether position model uses catenary equations, making the position estimate account for the curvature of the tether. The method is tested with a few static points and two outdoor flight tests, using RTK-GPS as a ground truth and position feedback. They are able to achieve an average error of $0.66\,\mathrm{m}$ at a tether length of about $5\,\mathrm{m}$. Most recently, Lima et al. [7] propose a classifier that chooses from three different models, a trigonometric (taut tether), a catenary (curving tether) and a neural network model according to the current state variables. Using custom built length, tension and angle sensors, the tether state variables are sensed. The Root Mean Square Error (RMSE) from the catenary model is about $1.27\,\mathrm{m}$ and the complete framework reports a RMSE of $1.1\,\mathrm{m}$.

Despite these advances, existing works have not reached localization accuracies that are sufficient for precise position control. Our work addresses this gap by introducing a catenary-based model corrected via a GP residual error prediction model. This enables real-time localization that is an order of magnitude more accurate than previous models. We provide analytical expression for the uncertainty as a function of sensor accuracies and tether state variables, and thoroughly validate our method in real experiments with variable tether lengths of up to $4.5\,\mathrm{m}$.

III. Tether-based Localization

The physical connection between the base and the drone generates a geometric constrain on the position of the drone in space: The drone can only be positioned at a location that is consistent with the tether state, allowing us to localize the TUAV. We choose to model the tether, as an idealized hanging chain. This assumes the shape of a catenary, first introduced by Leibniz, Huygens, and Bernoulli [10]. It is a model with four degrees of freedom and therefore requires four measurements to be uniquely identified. We choose the measurements of the tether length, the base elevation and azimuth angle, and the drone elevation angle. Furthermore, the catenary model relies on three main assumptions [11]:

i. The tether has negligible bending stiffness w.r.t. its weight
ii. The tether has a uniform mass distribution along its length

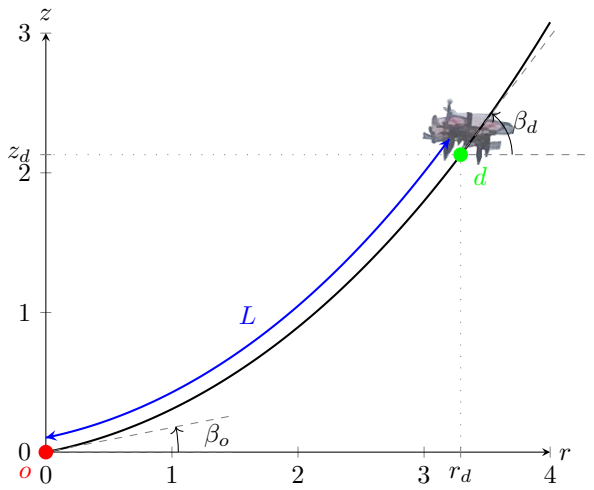

Fig. 2. 2D projection of the catenary problem showing state variables β_o, β_d, and L: elevation angles at origin and drone, and tether length, respectively. The azimuth angle α_o rotates this projected figure about the z-axis.

iii. The tether hangs between exactly two points in a uniform gravitational field

This limits the model to quasi-static conditions, whereas windy conditions and dynamic drone movement violate the model assumptions. To capture these model violations and other non-linear effects, we propose a data-driven approach. Using a dataset of ground truth positions and our catenary-based localization, we train a Sparse Gaussian Process [12] on the residual error.

A. Catenary Model

To simplify calculations, we consider the problem as planar. Within this plane we express the catenary curve as a following function that relates the radial distance (horizontal) with the Z-axis (upwards):

$$z(r) = a\cosh\left(\frac{r-b}{a}\right) + c \tag{1}$$

where a, b and c define the curvature and position of the catenary curve. At each timestep, to determine the position of the drone for some arc length of the curve, we need to find these unknown parameters from the measurement values, as well as the radial distance from the origin r_d which corresponds to the measured length. With the measurement values, the curve's base angle β_o, the endpoint angle β_d, and the curve's length L, displayed in Figure 2, we establish the following constraints:

$$z(0) = a\cosh\left(\frac{0-b}{a}\right) + c = 0 \tag{2}$$

$$\left.\frac{dz}{dr}\right|_{r=0} = \sinh\left(\frac{0-b}{a}\right) = \tan\beta_o \tag{3}$$

$$\left.\frac{dz}{dr}\right|_{r=r_d} = \sinh\left(\frac{r_d-b}{a}\right) = \tan\beta_d \tag{4}$$

$$L = \int_0^{r_d} \sqrt{1+(z'(r))^2}dr \tag{5}$$

Constraint (2) fixes the curve to pass through the origin. Constraints (3) and (4) ensure the curve slope matches the measured elevation angles at origin and drone positions. Constraint (5) enforces that the arc length equals the measured tether length. Taking the derivative of (1), substituting into (5), and integrating from 0 to r_d yields:

$$L = a[\sinh(\tfrac{r_d-b}{a}) - \sinh(\tfrac{0-b}{a})] = a(\tan\beta_d - \tan\beta_o) \tag{6}$$

This provides a in terms of known variables. We then solve for the remaining parameters, ultimately giving us (r, z_d), the coordinates of the drone in the projected 2D plane:

$$a = \frac{L}{\tan\beta_d - \tan\beta_o} \tag{7}$$

$$b = -a\sinh^{-1}(\tan\beta_o) \tag{8}$$

$$c = -a\cosh\left(\frac{b}{a}\right) \tag{9}$$

$$r_d = b + a\sinh^{-1}(\tan\beta_d) \tag{10}$$

$$z_d = a\cosh\left(\frac{r_d-b}{a}\right) + c \tag{11}$$

To go from the 2D projection to 3D coordinates, we need to rotate the planar solution by the azimuth angle α_o, finally yielding:

$$x_d = r_d\cos\alpha_o \tag{12}$$

$$y_d = r_d\sin\alpha_o \tag{13}$$

The closed-form solution enables real-time computation with minimal computational overhead, suitable for planetary exploration applications.

1) Model Uncertainty: As the catenary algorithm is a closed-form solution, the accuracy will depend on the measurement uncertainty of the variables that feed into the algorithm. By propagating the measurement error through our model, we can predict the impact of this error on the positional error. The sensors providing the azimuth and elevation angles are analog sensors, see section IV. This means the Analog-to-Digital Converter (ADC), the reference voltage and sensor imperfections introduce noise into the system. We determine the level of interference by measuring the standard deviations of the signals during static operation and deriving the partial derivatives w.r.t. each input variable to predict the impact of the sensor noise to a tether-localized position. Using some common definitions, to simplify the expressions,

$$\Delta = \tan\beta_d - \tan\beta_o \tag{14}$$

$$s_o = \sinh^{-1}(\tan\beta_o) \tag{15}$$

$$s_d = \sinh^{-1}(\tan\beta_d) \tag{16}$$

$$\Delta_s = s_d - s_o \tag{17}$$

$$A_o = \frac{\Delta}{|\cos\beta_o|} - \frac{\Delta_s}{\cos^2\beta_o} \tag{18}$$

$$A_d = \frac{\Delta}{|\cos\beta_d|} + \frac{s_o - s_d}{\cos^2\beta_d} \tag{19}$$

$$B = \frac{1}{|\cos\beta_d|} - \frac{1}{|\cos\beta_o|} \tag{20}$$

we yield the partial derivatives of x_d, y_d:

$$\frac{\partial x_d}{\partial L} = \frac{\Delta_s\cos\alpha_o}{\Delta} \qquad \frac{\partial y_d}{\partial L} = \frac{\Delta_s\sin\alpha_o}{\Delta} \tag{21}$$

$$\frac{\partial x_d}{\partial \beta_o} = -\frac{LA_o\cos\alpha_o}{\Delta^2} \qquad \frac{\partial y_d}{\partial \beta_o} = -\frac{LA_o\sin\alpha_o}{\Delta^2} \tag{22}$$

$$\frac{\partial x_d}{\partial \beta_d} = \frac{LA_d\cos\alpha_o}{\Delta^2} \qquad \frac{\partial y_d}{\partial \beta_d} = \frac{LA_d\sin\alpha_o}{\Delta^2} \tag{23}$$

$$\frac{\partial x_d}{\partial \alpha_o} = -\frac{L\Delta_s\sin\alpha_o}{\Delta} \qquad \frac{\partial y_d}{\partial \alpha_o} = \frac{L\Delta_s\cos\alpha_o}{\Delta} \tag{24}$$

and for z_d:

$$\frac{\partial z_d}{\partial L} = \frac{B}{\Delta} \tag{25}$$

$$\frac{\partial z_d}{\partial \beta_o} = \frac{L\left(-(\tan\beta_d\tan\beta_o+1)|\cos\beta_o| + \frac{1}{|\cos\beta_d|}\right)}{\Delta^2\cos^2\beta_o} \tag{26}$$

$$\frac{\partial z_d}{\partial \beta_d} = \frac{L\left(-(\tan\beta_d\tan\beta_o+1)|\cos\beta_d| + \frac{1}{|\cos\beta_o|}\right)}{\Delta^2\cos^2\beta_d} \tag{27}$$

$$\frac{\partial z_d}{\partial \alpha_o} = 0 \tag{28}$$

Intuitively, these show that within close proximity of the base, the length measurement has a larger influence on the uncertainty than the angle measurement, whereas at large tether lengths, the angle measurements contribute more to the estimate's uncertainty.

B. GP-Based Residual Error Compensation

During the experiments described in section V, all flight and tether data is captured. We use this data for training of a GP [12] to estimate the error between the tether-localized position and the ground truth position. We choose a GP to measure whether the current state lies within the training regime during operation using the variance of the Gaussian output. When this measurement is too high, we opt to scale down or completely disable the error compensation as the chance of catastrophic error estimation inaccuracies grows. We choose to scale the error compensation linearly according to the output variance of the GP. Through empirical tuning the lower threshold of $0.015\,\mathrm{m}$ and the upper threshold of $0.065\,\mathrm{m}$ are found. This provides safety guarantees and

TABLE I
MODEL PERFORMANCE COMPARISON WITH AND WITHOUT VARIANCE SCALER. MODEL 1 USES 1000 EPOCHS, ALL OTHERS 750 EPOCHS.

Model	Inducing Points	No Variance Scaler		Variance Scaler	
		Avg RMSE	Std Dev	Avg RMSE	Std Dev
No Model	-	0.1337	0.1211	-	-
Model 1	400	0.0836	0.1370	0.0783	0.1276
Model 2	400	0.0821	0.1348	0.0776	0.1270
Model 3	300	**0.0809**	**0.1331**	**0.0776**	**0.1255**
Model 4	500	0.0829	0.1365	0.0780	0.1283

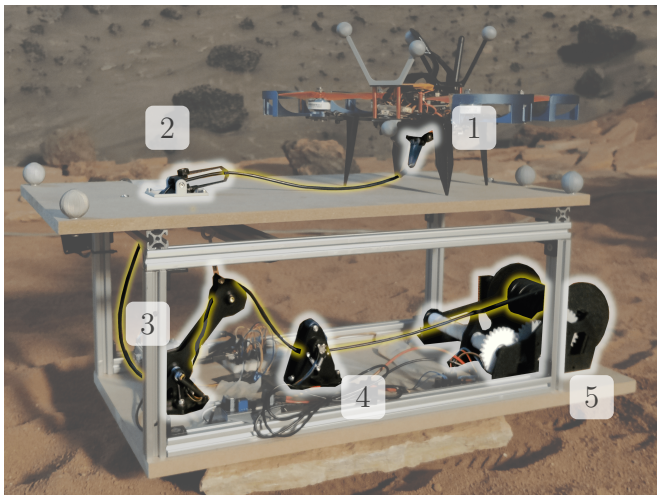

Fig. 3. The TMS that we developed where 1. & 2. highlight the drone and platform angle sensor, 3. is the tension sensor, 4. is the length sensor and 5. is the tether drum. The tether is highlighted in yellow.

enables us to test the GP in the closed-loop localization pipeline. The recorded experiment data contains all the relevant tether variables, the tether-localized position and the ground truth position. Using these we can form the input vector which consists of $\begin{bmatrix} x_d, & y_d, & z_d, & \alpha_o, & \beta_o, & \beta_d, & L \end{bmatrix}^\top$. The 3-dimensional output vector is defined as; $\mathbf{e}_d = \begin{bmatrix} x_{gt} - x_d, & y_{gt} - y_d, & z_{gt} - z_d \end{bmatrix}^\top$. As the experiment data contains 150k data points, it is necessary to sparsify this data due to poor scalability of GPs [13]. This is done using K-means clustering [14], where the final model is using 300 inducing points. The Adam optimizer [15] and the Evidence lower bound [16] is used for training the GP.

a) Hyperparameter Optimization: We conduct an ablation study to determine the impact of the number of inducing points and training epochs. The effectiveness of the model, measured with the average RMSE of each experiment, is tested on 30 different pre-evaluation flight experiments, where only 25 are used in our train/test/validation split. Table I shows that the RMSE and standard deviation grow with more inducing points. This is explained by overfitting, as trained flights perform better but unseen flights perform significantly worse using more inducing points.

TABLE II
A RANDOMLY SAMPLED FLIGHT DATA POINT WITH SENSOR UNCERTAINTY COMPUTED FROM THE STANDARD DEVIATION OVER A 10 s TIME WINDOW.

	α_o (rad)	β_o (rad)	β_d (rad)	L (m)
Sample	1.774	0.841	1.117	4.284
Std. Dev. σ	$\pm$0.0005	$\pm$0.0096	$\pm$0.026	$\pm$0.003

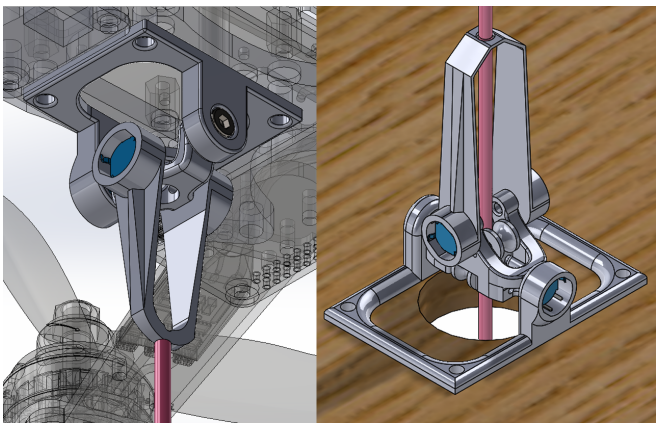

Fig. 4. The drone angle sensor with the red tether attached (left) and the platform angle sensor with the red tether passing through (right).

IV. SYSTEM DESIGN

This section details our design and fabrication of the TMS and the accompanying sensor suite, both developed by us specifically to support the localization pipeline. A crucial part, as the precise fabrication allows for low sensor uncertainties that directly contribute to position uncertainties. The integrated system fulfills two primary functions:

i. Collecting tether state variables (α_o, β_o, β_d, and L) required for localization
ii. Managing tether length and tension to prevent entanglement while preserving drone mobility within the maximum tether radius.

To isolate the localization problem, the current implementation does not include data or power transfer between the platform and the drone.

A. Tether Angle Sensors

Employed at position 1 and 2 of the TMS in Figure 3, the angle sensors measure the elevation and azimuth of the tether relative to both the drone and platform vertical axes. As shown in Figure 4 both sensors employ a two-axis gimbal design with low-friction potentiometers on each axis, designed by us and partially inspired by Lima et al. and Borgese et al. [9, 17]. The platform-mounted sensor allows the tether to traverse both rotation axes before entering the TMS. To reduce friction at low angles – i.e. when the tether lays almost horizontal – this sensor incorporates small rollers (7.5 mm diameter) mounted on metal pins. The last linkage of both sensors is designed to be lightweight to minimize the moving mass of the angle

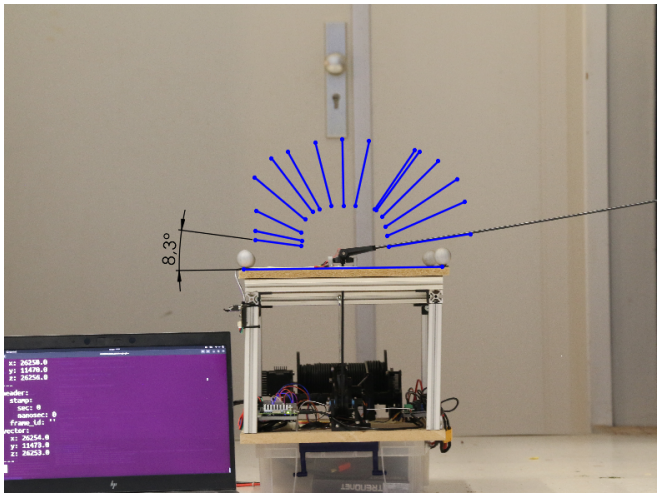

Fig. 5. Calibration photo with the overlay of all the angle sensor angle samples. The laptop on the left is displaying its current sensor values.

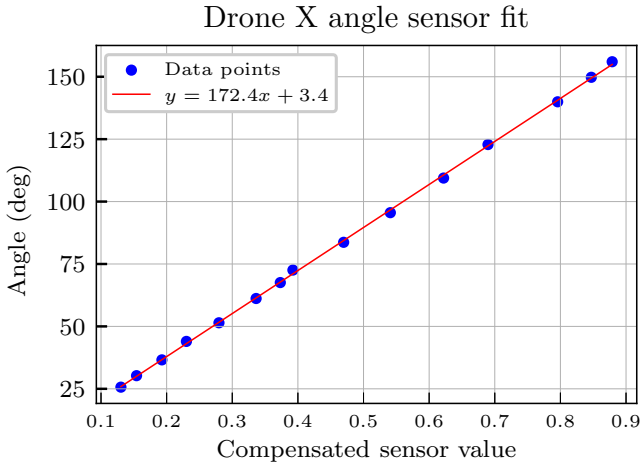

Fig. 6. Calibration curve fit of the drone angle sensor, resulting in a linear function from Analog-to-Digital Converter (ADC) value to angle. The blue dots are the samples and the line is the function.

sensor, minimizing tether deformation due to angle sensor interaction.

Both sensors are calibrated by taking orthographic pictures in-line with the axis while moving the tether in the axis plane. The value of the ADC potentiometer and the value of the ADC reference voltage are also captured in the frame, which can be seen in Figure 5. The reference voltage value is used to account for any fluctuation in the reference voltage, which is crucial for the drone angle sensor, since the supply voltage fluctuates heavily during flight. Using these pictures we can determine which angle corresponds to which sensor value, allowing us to determine the linear fit between sensor values and tether angles. One of these fits is shown in Figure 6. Using the drones attitude extracted from its Inertial Measurement Unit (IMU), the system compensates the sensed tether angle, such that the output tether angle is always w.r.t. the horizon.

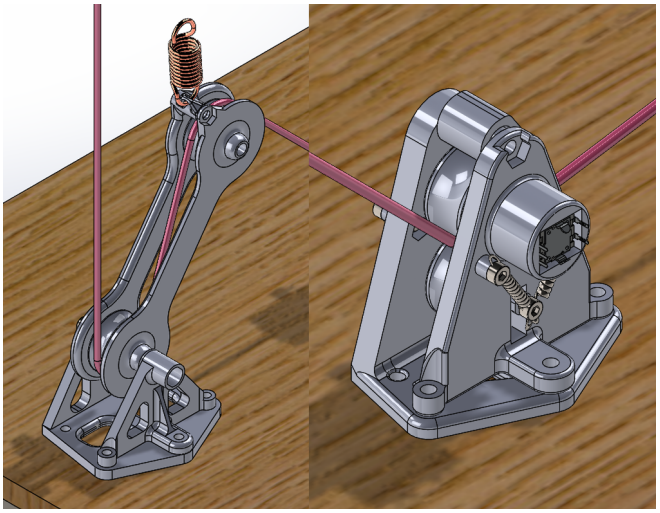

Fig. 7. The tension sensor on the left and the length sensor on the right with the red tether moving through their rollers. The spring of the tension sensor is attached to the underside of the landing platform. The shaft of the bottom roller of the length sensor is actuated by the two springs on both sides.

B. Tether Length Sensor

The length sensor (position 4 in Figure 3) uses a dual-roller system where the upper roller connects to a rotary encoder and the lower roller operates on a spring-actuated shaft. In Figure 7, it can be seen that two lateral springs create pinching force against the upper roller, preventing slippage and ensuring accurate length measurement. Although this measurement could alternatively be obtained by attaching an encoder directly to the tether drum, such an approach would introduce uncertainty due to variations in the effective drum radius as the tether is wound and unwound. This design also functions as a guide pulley, directing the tether from the variable tension sensor position to the fixed drum location. The calibration procedure is quite simple, as the drone is positioned on the platform while attached to the tether, and the encoder count is reset to zero. The drone is then systematically moved to increasing distances from the platform, with each position measured using a laser rangefinder. The collected encoder readings and corresponding distance measurements are used to fit a calibration curve, as demonstrated in Figure 8.

We evaluate the sensor standard deviation in static conditions in order to use these uncertainties with the partial derivatives from paragraph III-A1. We report the results in Table II. We then take 3000 random data points and compute the estimation error. We also sample from the ideal state-dependent distribution using is convariance matrix $\mathbf{\Sigma}_{\text{output}}$ computed via:

$$\mathbf{\Sigma}_{\text{output}} = \mathbf{J}\mathbf{\Sigma}_{\text{input}}\mathbf{J}^{\top} \tag{29}$$

with $\mathbf{J}$ being the Jacobian of the estimation output with respect to the sensor input (i.e., the collection of the partial derivatives in Equations (21) to (28)) and $\mathbf{\Sigma}_{\text{input}}$ denoting the input covariance matrix. As shown in Figure 9 these distributions

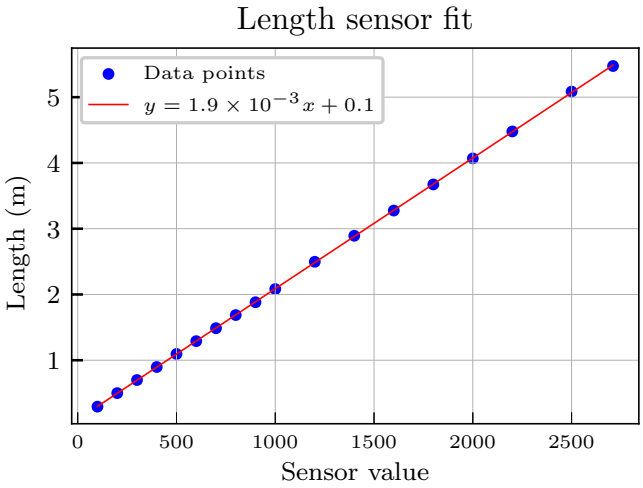

Fig. 8. The length sensor calibration shows a linear relationship between encoder counts and tether length. Each blue dot represents a sample combining laser-measured platform distance with the corresponding encoder value.

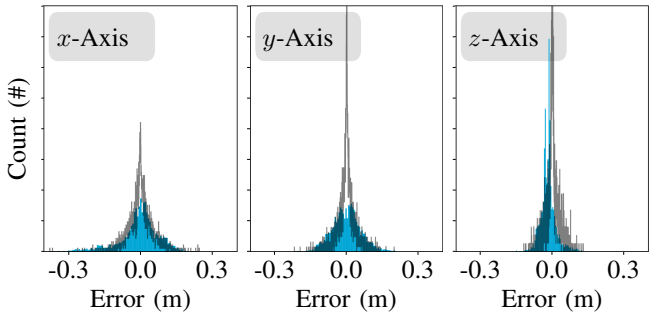

Fig. 9. Empirically observed (blue) and predicted (black) error distribution across 3000 samples for all estimation axes. The distributions clearly overlap, with only minor offsets in the z-axis, showing the accuracy of our uncertainty prediction.

mostly overlap, with only the z-Axis showing a small bias to underestimate the height.

Finally, the tether selection employs a highly flexible silicone-insulated cable to approximate the catenary model assumptions while providing sufficient mass to overcome sensor friction. We calculate the minimum required tether density based on the measured static angle sensor friction of $0.029\,\mathrm{N}$ per sensor axis. We assume a minimum tether length of $0.2\,\mathrm{m}$ to calculate how much force the tether can enact on the angle sensor on one side, accounting for scenarios of double this length. This only takes the weight of the tether into account, ignoring any tension, leading to an overestimate of the required density. This is not a problem however, as long as the total tether weight is still within the maximum payload

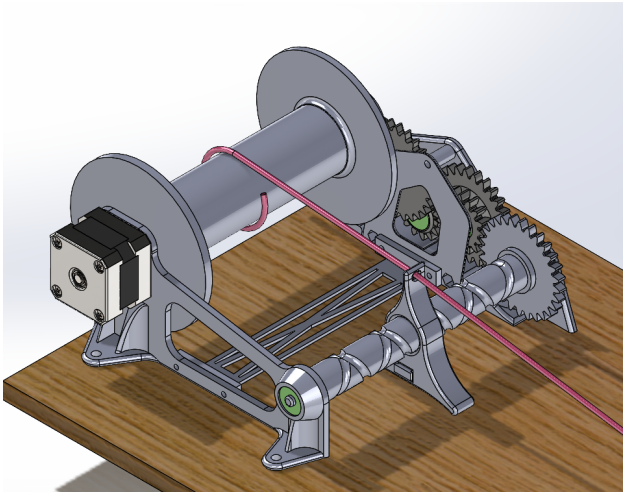

Fig. 10. The tether drum assembly featuring a self-reversing leadscrew mechanism for uniform tether winding, driven by a stepper motor through a 7.5:1 gear reduction.

specification of the drone.

$$0.003\,\mathrm{kg} \cdot 9.81\,\mathrm{m/s^2} = 0.029\,\mathrm{N} \tag{30}$$

$$0.029\,\mathrm{N} = \rho \cdot L \cdot g \tag{31}$$

$$\frac{0.029\,\mathrm{N}}{L \cdot g} = \rho = 15\,\mathrm{g/m} \tag{32}$$

In this prototype we will use a highly flexible silicone insulated tether of $22\,\mathrm{kg/km}$. This corresponds with commercially available drone tethers, for example a 5-core power and data cable by GORE [18].

C. Tether Management

The tether drum assembly (position 5 in Figure 3) incorporates a system with a self-reversing leadscrew mechanism indirectly driven by the stepper motor through a 7.5:1 gear reduction. This leadscrew provides uniform tether distribution across the drum width, preventing bunching and ensuring consistent operation, which can be seen in detail in Figure 10. The tension sensor is designed with a spring-actuated arm (position 3 in Figure 3) that pivots around a lower axis with the upper end connected to a spring, inspired by Lima et al. [7]. As tether tension increases, the arm rotates downward, with angular displacement measured via a potentiometer. This sensor is calibrated utilizing a spring balance across the $0\,\mathrm{N}$ to $6\,\mathrm{N}$ range, establishing a quadratic relationship between potentiometer readings and tension, as shown in Figure 11.

D. Controller

A Proportional-Derivative (PD) controller maintains tether tension at $3.5\,\mathrm{N}$, determined empirically to balance drone mobility with system sensitivity, as initial testing revealed that a low setpoint value could result in false tension readings when angle sensor friction increased, masking the actual tether tension. The controller uses a low-pass filter for noise attenuation and implements a quadratic proportional term:

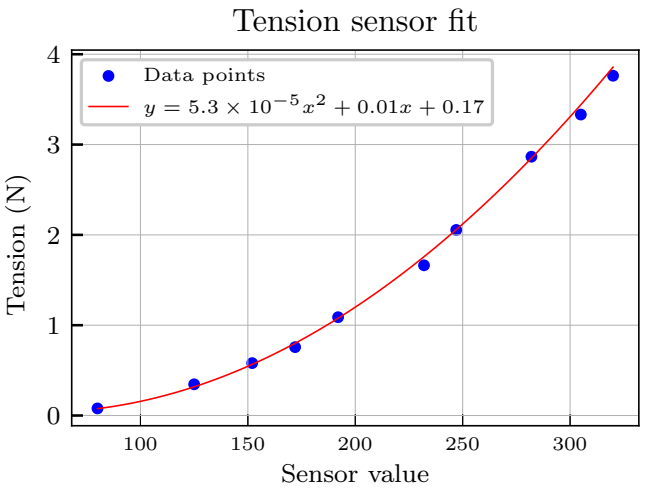

Fig. 11. Tension sensor calibration showing the quadratic relationship between potentiometer readings and measured tension. Each blue dot represents a calibration point combining spring balance measurements (in Newtons) with corresponding potentiometer values.

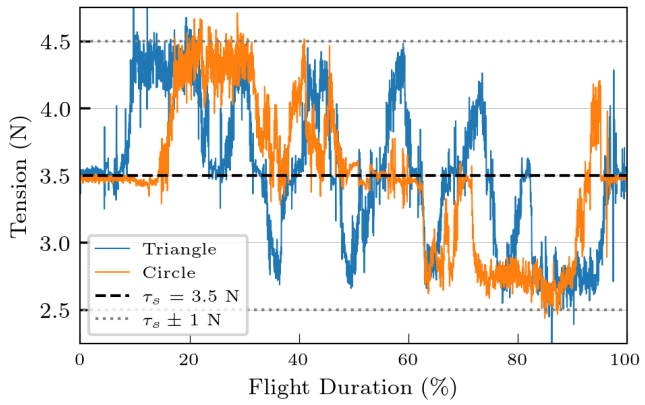

Fig. 12. The tether tension for a triangular and circular flight experiment and its reference value τ_s, regulated by the tension controller (Equation 33) throughout a flight experiment. The controller successfully tracks the setpoint without causing large oscillations, staying within the reactivity threshold ± 1 N. The inflection points of the triangular flights can be seen causing extremes in tension.

reduced sensitivity for small deviations (<1 N) and enhanced responsiveness for larger deviations (>1 N), as below:

$$\omega = k_P(\tau_s - \tau)|\tau_s - \tau| - k_D\dot{\tau} \tag{33}$$

where ω is the motor speed, k_P and k_D are the proportional and derivative gains, τ_s and τ are the tension setpoint and value. This prevents oscillatory behaviour while ensuring rapid response to significant tension changes as shown in Figure 12.

E. Communication

The hardware architecture, shown in Figure 13, provides the computational framework necessary for TI localization and active control of tether tension and length. The system

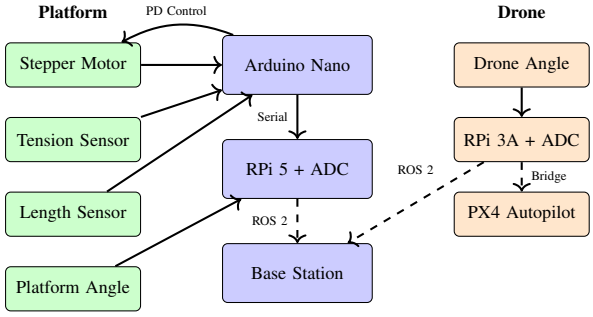

Fig. 13. Hardware architecture showing the distributed computing system with Arduino handling motor control and sensor data, Raspberry Pi 5 managing platform communications via ROS 2, and drone-mounted Raspberry Pi 3A interfacing with the autopilot system.

employs a distributed computing approach consisting of an Arduino Nano interfaced with the stepper motor, tension sensor potentiometer, and length sensor encoder. The Arduino communicates with a Raspberry Pi 5 via serial connection to broadcast platform state information to the Robot Operating System (ROS) 2 network. The Raspberry Pi incorporates an additional ADC module to acquire angle sensor potentiometer values, which are subsequently distributed through the ROS 2 communication framework. The separate ADC configuration was implemented due to accuracy limitations of the Arduino's integrated ADC, particularly regarding reference voltage stability. Since angle sensor output represents a percentage of the reference voltage, any noise generated by the stepper motor driver would propagate directly to the angle measurements. The drone incorporates a Raspberry Pi 3A as a companion computer, interfacing with an additional ADC and the PX4 Autopilot system. This configuration enables the drone-mounted Raspberry Pi to collect angle sensor data while maintaining communication bridges between the base station and the flight controller.

The complete data acquisition pipeline culminates at the base station, where all sensor readings are processed to calculate tether geometry and, subsequently, drone position. The base station transmits the tether estimated postion and the flight path, where the autopilot system integrates tether-derived position estimates with IMU data.

F. System Integration

The system is integrated within a framework constructed from 20mm aluminum extrusions, with wooden fibreboards for the base and top platforms. All sensor components are mounted to these boards, with mounting hardware for the control electronics including an Arduino microcontroller and Raspberry Pi 5 with an ADC, as can be seen in Figure 3.

The top platform incorporates a designated landing area where the drone can take-off and land either directly above or next to the angle sensor. Both the platform and drone are equipped with VICON motion capture markers to enable ground-truth data collection for validation of the TI localization methodology.

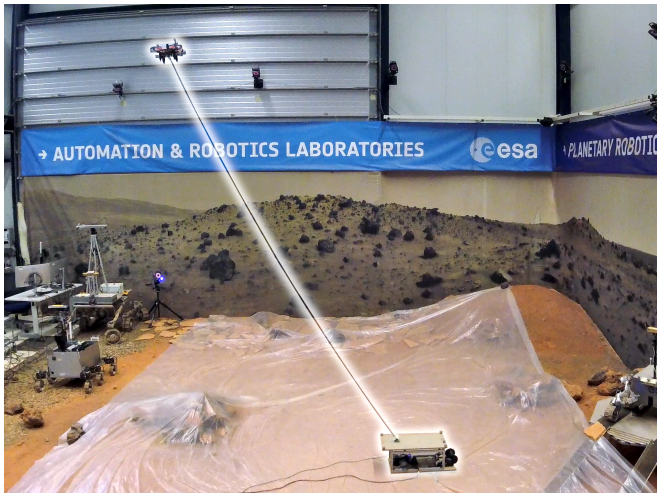

Fig. 14. Localization experiment in the Planetary Robotics Lab at ESA ESTEC, with the TMS and the TUAV highlighted.

V. Experiments

To evaluate the performance of the proposed drone–rover TI localization approach, comprehensive flight experiments were conducted using a custom TMS and a HolyBro QAV250 quadrotor in the PRL at ESA, ESTEC, as shown in Figure 14.

A. Experimental Setup

A VICON motion capture system provides ground truth positioning data, constraining the operational height to approximately $4.5\,\mathrm{m}$ due to camera coverage limitations. However, please note that the motion capture system is only used for ground truth comparison and the drone's position feedback is solely supplied by our TI Localization framework. All results presented are the raw results before merging with the inertial odometry in the Extended Kalman Filter (EKF) of the drone. The experimental campaign comprises of 19 flight missions totaling 41 minutes of flight data across three distinct trajectory geometries: circular, triangular, and figure-eight patterns. We evaluate two altitude configurations: flights at $2.0\,\mathrm{m}$ height with $1.5\,\mathrm{m}$ characteristic dimensions (radius for circles, side length for triangles), and flights at $3.5\,\mathrm{m}$ height with $2.5\,\mathrm{m}$ characteristic dimensions. The tether's maximum length varies between $3\,\mathrm{m}$ and $4.5\,\mathrm{m}$ for the different sizes, respectively. This systematic variation allows the assessment of both altitude and scale effects on localization accuracy. Each flight mission followed a standardized protocol:

i. Vertical takeoff to the target altitude
ii. Autonomous following of the prescribed trajectory
iii. Descent back onto the platform.

The drone's position controller uses the TI Localization for 12 flights, and the GP-enhanced variant for 7.

B. Results

Table III displays the estimation RSME over all trajectories. Hereby, we point out the difference between raw TI estimation and GP-enhanced estimation. Across all experiments, we show

TABLE III
Localization Performance Comparison Across Trajectories and Estimation Modes. The average, the worst, and the best performances are highlighted in the last column in bold.

Shape	Size (m)	Source	QTY	Duration (min)	Avg RMSE (m)
All	All	TI	12	27.0	**0.073**
All	All	GP	7	14.0	**0.049**
Circle	3	TI	9	12.7	0.057
	4.5	TI	3	7.5	0.093
	3	GP	1	1.8	0.040
	4.5	GP	1	2.0	0.064
Eight	3	TI	2	3.2	0.063
	4.5	TI	1	2.1	**0.140**
	3	GP	2	3.4	0.056
	4.5	GP	1	2.0	0.110
Triangle	3	TI	1	2.3	0.054
	4.5	TI	2	4.5	0.078
	3	GP	1	2.3	**0.022**
	4.5	GP	1	2.6	0.057

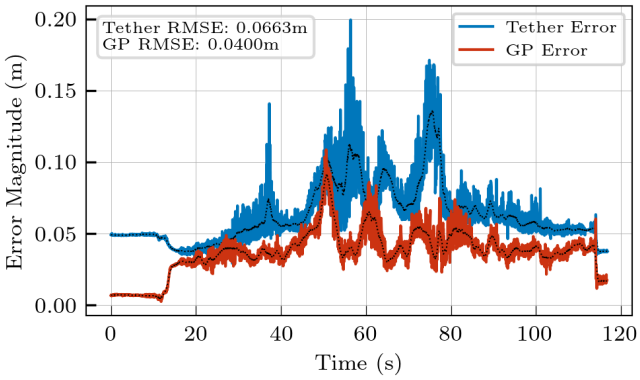

Fig. 15. The magnitude of positional error using TI localization and GP compensated error during a circle flight experiment of 2m high.

that the raw TI position estimation achieves accuracies in the range of $10\,\mathrm{cm}$. Performance is better for trajectories with smaller characteristic dimensions, as shown in Equations (21) to (28): the uncertainty scales linearly with the tether length L which increases with characteristic dimension. Furthermore, we demonstrate the the GP improves performance across all trials achieving average RMSEs up to $2.2\,\mathrm{cm}$. The overall improvement from TI localization (0.073 m average RMSE) to the GP-enhanced TI system (0.049 m average RMSE), represents a 33% decrease of RMSE over the analytical model. Figure 15 shows this exemplary for an individual flight. The GP decreases the estimation error across the entire flight. Especially at approximately time $58\,\mathrm{s}$ we observe the GP compensating a large error spike in the raw TI showcasing its capability to compensate for unmodeled effects.

Similarly, Table IV shows the influence of trajectory ge-

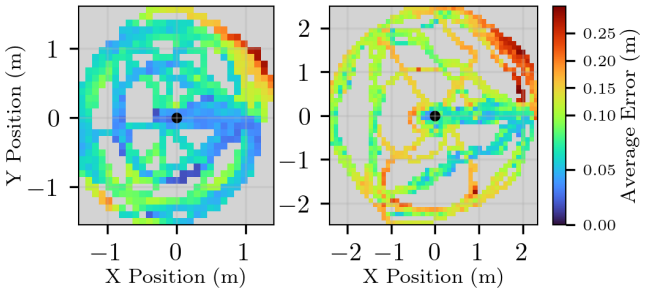

Fig. 16. A top-down view of the average error for every 0.10m square around the origin (black). Left is the average error for flights of 1.5m characteristic dimension and right is for flights with a 2m dimension. Grey indicates that there are no samples in the voxel.

TABLE IV
LOCALIZATION ACCURACY BY TRAJECTORY GEOMETRY AND SCALE

	Avg RMSE ± Std Dev (m)	
Trajectory	Small Scale (2m)	Large Scale (3.5m)
Circle	0.052 ± 0.014	0.080 ± 0.014
Figure Eight	0.057 ± 0.001	0.126 ± 0.021
Triangle	0.042 ± 0.018	0.065 ± 0.006

ometry and scale on localization accuracy. In particular, it shows that larger trajectory dimensions consistently increase localization error across all geometries. However, the system is able to provide localization estimates that are sufficient for position control in all cases. The same trend can be observed in Figure 16, which displays the mean error for $10\,\mathrm{cm}$ voxels in the horizontal plane. We observe error prone regions for the small and larger test flights that are concentrated particulary for large positive x and y positions. It becomes especially clear in the right plot that the angle sensors deviate in the positive XY direction, sometimes causing errors of up to $0.30\,\mathrm{m}$. This indicates a biased systematic error in one side of angle sensor. Lastly we want to showcase tether configurations that introduce technical difficulties for state estimation. Figure 17 illustrates one trial for the three selected trajectories respectively, with position error magnitude color-coded relative to the ground truth position (shown in black). Notable deviations from the ground truth occur primarily at trajectory inflection points, particularly evident in the triangular pattern following sharp corners. This behavior results from the low bandwidth of the tether tension controller, which requires a minimum amount of time to reconverge to the appropriate tension. In the transient phase, which correlates with the trajectory inflection points, overcoming the angle sensor friction becomes increasingly difficult as tether tension drops. This violates the catenary assumptions as effectively, the end of the angle sensor acts as a new anchor point until the friction can be overcome. The figure-eight trajectory exhibits the most challenging dynamics for the tether management system, requiring two rapid reductions in tether length per cycle where we can observe this behaviour. Hereby, tether tension reduces below the $3.5\,\mathrm{N}$ setpoint, causing momentary degradation in angle sensor accuracy as the tether approaches slack conditions.

VI. CONCLUSION

This work presents a drone-rover tether-inertial localization pipeline for precise positioning of tethered UAVs. In environments that are GNSS-denied or where other estimation approaches such as visual inertial odometry struggle this works provides a viable alternative. The approach combines a computationally efficient analytical catenary model with Gaussian Process error compensation to achieve accurate real-time localization, rigorously tested on an custom developed TMS, while also providing uncertainty guarantees from the sensor accuracies. The analytical catenary model provides closed-form solutions for drone position estimation using tether state measurements. These tether state measurements are supplied by a our custom TMS deployed together with our customized drone. Experimental validation demonstrated an average RMSE of $0.073\,\mathrm{m}$ across 27 minutes of flight time. These test flights where conducted by flying circular, triangular, and figure-eight trajectories autonomously. The integration of GP compensation reduced localization error by 33%, achieving an average RMSE of $0.049\,\mathrm{m}$ over 14 additional minutes with variance-based confidence scaling. The demonstrated localization accuracy of approximately $5\,\mathrm{cm}$ represents a significant improvement over existing TUAV localization methods and enables autonomous flight operations in feature-sparse environments, such as planetary surfaces.

In future work we intend to extend the estimation methodology to also infer the heading of the TUAV using a orthogonal angle sensor at the anchor point of the drone for an added degree of freedom. Besides state estimation, we believe work on the control algorithm of the TUAV could lower positional error further, as experiments in this work have been conducted using the default positional controller of the UAV. A controller that accounts for the tether tension force direction and magnitude will be better suited, as this will increase path following accuracy. Aside from better path following, the TUAV will also experience less turbulence, which results in a more stable tether, which in turn benefits the position estimation accuracy. Further experimental validation in dynamic scenarios could also indicate safety limits of drone velocity. This experimentation data can be used for incorporating a tether dynamic model to provide estimates of the UAV velocities and to compensate any positional error generated by the oscillation or mass inertia of the tether, as these violate the constraints of the catenary model. Furthermore, research into robust, small and space-ready hardware with rigorous experimental validation will enable us to integrate the TMS on a rover with active tether control, where the drone and TMS cooperatively regulate the tether length without the need of tether tension feedback. This will create a powerful rover-drone system that is suitable for difficult planetary exploration tasks.

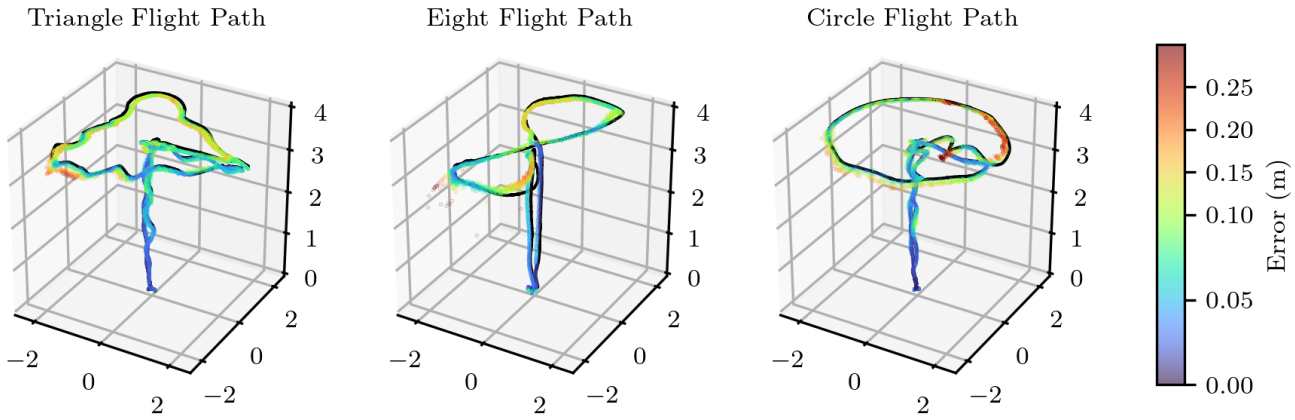

Fig. 17. Different flight shapes used in the experiments. The tether-localized position is plotted in colour according to the position error w.r.t. the ground truth flight path, which is plotted in black.

References

[1] Nicolas Mangold et al. "Perseverance rover reveals an ancient delta-lake system and flood deposits at Jezero crater, Mars". In: *Science* 374.6568 (2021), pp. 711–717.

[2] J Balaram, MiMi Aung, and Matthew P Golombek. "The ingenuity helicopter on the perseverance rover". In: *Space Science Reviews* 217.4 (2021), p. 56.

[3] DC Agle. 2024. URL: https://www.jpl.nasa.gov/news/nasa-performs-first-aircraft-accident-investigation-on-another-world/.

[4] Samuel O Folorunsho and William R Norris. "Redefining aerial innovation: Autonomous tethered drones as a solution to battery life and data latency challenges". In: (2024). eprint: 2403.07922 (cs.RO).

[5] Amer Al-Radaideh and Liang Sun. "Self-Localization of Tethered Drones without a Cable Force Sensor in GPS-Denied Environments". In: *Drones* 5.4 (2021). ISSN: 2504-446X.

[6] Marco Tognon. "Theory and Applications for Control and Motion Planning of Aerial Robots in Physical Interaction with particular focus on Tethered Aerial Vehicles". Theses. INSA de Toulouse, July 2018.

[7] Rogerio R Lima and Guilherme A S Pereira. "A multi-model framework for tether-based drone localization". en. In: *J. Intell. Robot. Syst.* 108.2 (June 2023).

[8] Xuesu Xiao et al. "Indoor UAV Localization Using a Tether". In: *2018 IEEE International Symposium on Safety, Security, and Rescue Robotics (SSRR)*. 2018, pp. 1–6.

[9] Andrea Borgese et al. "Tether-Based Localization for Cooperative Ground and Aerial Vehicles". In: *IEEE Robotics and Automation Letters* 7.3 (2022), pp. 8162–8169.

[10] Leonhard Euler. *The rational mechanics of flexible or elastic bodies 1638-1788: introduction to Vol. X and XI*. Springer Science & Business Media, 1980.

[11] E H Lockwood. *Book of Curves*. Cambridge, England: Cambridge University Press, Dec. 2007.

[12] Carl Edward Rasmussen and Christopher K I Williams. *Gaussian processes for machine learning*. en. Adaptive Computation and Machine Learning Series. London, England: MIT Press, June 2005.

[13] Mitchell McIntire, Daniel Ratner, and Stefano Ermon. "Sparse Gaussian processes for Bayesian optimization." In: *UAI*. Vol. 16. 2016, pp. 517–526.

[14] Abiodun M. Ikotun et al. "K-means clustering algorithms: A comprehensive review, variants analysis, and advances in the era of big data". In: *Information Sciences* 622 (2023), pp. 178–210. ISSN: 0020-0255.

[15] Remi Genet and Hugo Inzirillo. *CaAdam: Improving Adam optimizer using connection aware methods*. 2024. arXiv: 2410.24216 [cs.LG].

[16] Alexander Alemi et al. "Fixing a broken ELBO". In: *International conference on machine learning*. PMLR. 2018, pp. 159–168.

[17] Rogerio Rodrigues Lima. "Exploiting the Advantages and Overcoming the Challenges of the Cable in a Tethered Drone System". PhD thesis. West Virginia University Libraries, 2023.

[18] W. L. Gore and Associates. 2024. URL: https://www.gore.com/system/files/2024-01/GORE-AD-TDrone-Data-Sheet-US-Jan24.pdf.

[This page is intentionally left blank]

Part III

Literature Review

The State of the Art of Drone State Estimation

A literature review

by

Dielof van Loon

Student No.
5346894

Daily Supervisor:	A. Bredenbeck, L. Puck
Supervisor:	S. Hamaza, J.M. Prendergast
Project Duration:	December, 2024 - November, 2025
Department:	Cognitive Robotics
Faculty:	Faculty of Mechanical Engineering, Delft

Cover: Tethered Drone Experimentation in the Planetary Robotics Lab at ESA, ESTEC. ESA-SJM Photography (ESA Standard Licence).

TU Delft

Abstract

Unmanned Aerial Vehicles (UAVs) designed for Martian environments require accurate and robust localization, as failures can be catastrophic for expensive exploration missions. Global Navigation Satellite System (GNSS) is unavailable on Mars, while vision-based localization methods suffer from computational constraints, drift accumulation, and failures in featureless terrain, demonstrated by the Ingenuity helicopter crash. This literature review assesses conventional localization techniques and reviews tether-based positioning as an alternative localization method for Tethered Unmanned Aerial Vehicles (TUAVs) paired with rovers.

The performance of conventional methods, like GNSS or visual odometry-like methods, are analyzed in view of Size, Weight, and Power (SWaP) budgets and reliability. The review then surveys tether-based localization methods, identifying two genres, namely trigonometric and catenary models. Taut-tether methods are more accurate with positioning errors of $0.23\,\mathrm{m}$ to $0.3\,\mathrm{m}$, but require high tension ($4\,\mathrm{N}$ to $20\,\mathrm{N}$), which grows with larger cable lengths, detrimental to payload capacity and power consumption of drones. Catenary-based works can model longer tethers at reduced tension but unfortunately demonstrate higher errors ($0.37\,\mathrm{m}$ to $1.1\,\mathrm{m}$), which is primarily attributed to sensor inaccuracies rather than model limitations. The review identifies research gaps such as insufficient error analysis, custom hardware without systematic validation and lack of residual error compensation strategies. Future work should look into development of reliable fully instrumented test platforms, identification of error sources and learning-based residual error compensation to achieve the positioning accuracy required for autonomous flight control in planetary exploration missions.

Contents

1

Introduction

The growing focus on planetary exploration for applications like resource extraction and habitability assessment relies on the development of increasingly sophisticated autonomous systems. Recent examples feature the Perseverance rover [1] and the Ingenuity helicopter [2], which proved the viability of UAVs on Mars. Aerial robots can significantly enhance mission performance by mapping terrain, detecting distant objects, and collecting data from vantage points inaccessible to ground-based rovers.

Despite these successes, a fundamental challenge for any autonomous mobile robot is robust and accurate localization. UAVs typically rely on conventional techniques such as the GNSS for outdoor navigation on Earth, or on-board sensor suites for Visual Inertial Odometry (VIO) in environments where GNSS is unavailable. However, these established methods face significant limitations in planetary exploration contexts. Highly accurate GNSS is, of course, unavailable on Mars. This necessitates reliance on other sensors, such as VIO technologies. VIO estimates motion by tracking features in the environment, but is critically vulnerable in the visually degraded and feature-sparse terrain common on other planets, such as vast stretches of sand. This very issue led to the conclusion of the Ingenuity mission, which ended in a crash caused by insufficient features for its vision-based localization system [3], as can be recognized in the bland landscape pictured in Figure 1.1. Furthermore, the strict payload constraints of small UAVs, also known as their SWaP budgets, limit the compute and power available for flying and processing sensor data.

One promising approach to mitigate these challenges is the use of a TUAV connected to a rover. A physical tether offloads the critical issues of battery endurance and limited computational capability to the base platform, where these do not affect weight and size limitations. TUAV systems are already being deployed in a variety of applications that require extended flight duration [4] and reliable communication links, including surveillance [5], infrastructure inspection [6, 7], and defense operations [8].

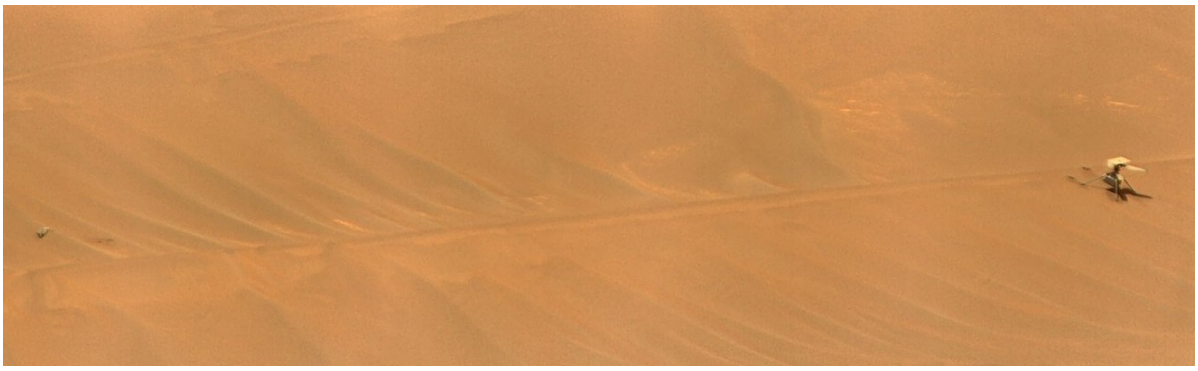

Figure 1.1: Ingenuity crash site at the sand dunes of Mars, featuring bland and featureless terrain presenting an obstacle to Visual Odometry localization algorithms. [2]

However, few systems exploit the physical properties of the tether itself (such as its length and angles) as a primary sensing modality for localizing the UAV relative to its base. While some tether-based localization methods exist, existing works have generally not achieved the accuracy required for precise position control, often reporting errors of $0.3\,\mathrm{m}$ or more. This review aims to survey the limitations of conventional localization and the current state-of-the-art in tether-based methods to identify the most promising approaches for achieving high-accuracy positioning.

1.1. Research Question

To achieve this goal, this review aims to answer the following research question:

> *To what extent can tether-based localization systems for UAVs mitigate the performance limitations of conventional UAV pose estimation in the context of planetary exploration?*

Where a *planetary exploration setting* is defined as a GNSS-denied and visually challenging (e.g., feature-sparse or unfamiliar) environment. To provide a structured answer to this main question, the following sub-questions will be addressed:

1. *What are the primary performance limitations of conventional UAV localization techniques in the context of planetary exploration?*
   This is answered in chapter 2, which details the trade-offs of current localization strategies.
2. *How have tether-based models been implemented for tethered UAV localization, and what is their state-of-the-art performance in terms of accuracy, robustness, and computational complexity?*
   This is answered in chapter 3, where the latest works in tether-based positioning are discussed.

2

Challenges in Conventional UAV Localization

2.1. Global Navigation Satellite System (GNSS)

GNSS methods are among the most popular for absolute UAV localization, as they can directly provide a position estimate in a global reference frame. Each GNSS receiver uses signals from four or more satellites to trilaterate its position using the signal's travel time. For a more accurate position estimate, differential techniques like Real-Time Kinematic (RTK) or correction services like Precise Point Positioning (PPP) can be used.

RTK uses an additional ground station as a reference [9], increasing precision to the sub-centimeter level but also narrowing its operational range, as the base station must be relatively close. However, due to their high precision, update rate, and reliability, RTK systems are widely used in agriculture [10] and for monitoring landslides, bridges, buildings, and infrastructure [11].

PPP [12] uses model-based error compensation by applying precise information on satellite orbits, clock errors, and atmospheric effects. Retrieving these corrections adds a layer of complexity, and the initialization of PPP often takes tens of minutes as its ambiguity resolution converges [13]. For single-constellation PPP, a realistic achievable accuracy is in the sub-meter range [14].

As the name suggests, GNSS performance depends on its space infrastructure. As satellites are obstructed from view, position estimates will start to diverge, degrading the performance of error compensation algorithms like PPP. To combat this problem, multiple works investigate the use of hybrid solutions, where drones fall back on other sensors, integrating their translational estimates with the last known GNSS position. This also mitigates long PPP reconvergence periods, which can be critical as the drone temporarily loses position awareness. Chi et al. [14] address this during a complete $10\,\mathrm{s}$ GNSS outage in an open-sky environment using Inertial Measurement Unit (IMU) data, improving the positional Root Mean Square Error (RMSE) from $0.93\,\mathrm{m}$ to $0.039\,\mathrm{m}$. Wang et al. [15] add visual data to perform VIO in tandem with GNSS while driving through streets with high-rises and achieve a positional RMSE of $0.13\,\mathrm{m}$, while the GNSS-only method achieves a RMSE of $2.35\,\mathrm{m}$ as satellites are blocked.

Unfortunately though, space localization infrastructure is not available on other planets. As lunar missions are relatively close by, compared to Mars, successful experiments have been done to try and capture GNSS signals on the Moon [16], but highly accurate localization will still be a challenge as limited signal is available. As the distance to Mars is so great, using a GNSS concept would only be feasible by placing four or more satellites into orbit around Mars, which would be a costly and ambitious endeavor.

2.2. Vision-Based Localization

In environments where GNSS is unavailable or unreliable, such as subterranean, dense urban, or extraterrestrial settings, alternative localization strategies are required. Vision-based localization, which leverages cameras and inertial sensors, provides a self-contained solution for ego-motion estimation. This process, known as odometry, incrementally computes the UAV's trajectory relative to its starting position by analyzing the motion of the environment in video feeds. Visual Odometry (Visual Odometry (VO)) and Visual-Inertial Odometry (VIO) systems can be categorized based on several key design choices regarding their sensor modality, algorithmic approach to motion estimation, and optimization techniques.

Direct vs. Feature-Based Methods The core of a VO pipeline is the method used to estimate motion between camera frames. These methods are broadly classified as either feature-based (indirect) or direct. **Feature-based methods**, used in earlier algorithms, operate by first detecting and describing features, such as corners or blobs, within an image, as seen in Figure 2.1. These features are then matched across consecutive frames, recovering the UAV's motion by minimizing a geometric reprojection error, which is the discrepancy between the observed feature locations and their predicted locations based on an estimated camera pose and 3D feature points. This optimization is well-known as the Perspective-n-Point (PnP) problem [17, 18, 19].

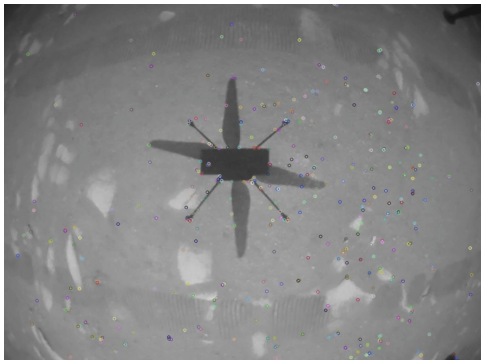

Figure 2.1: Image from the VO camera from the Ingenuity helicopter, showing the selected features in frame [2].

Recent advances in feature selection have shifted to **learning-based methods** [20, 21], instead of geometric features. However, these selectors still often prefer classical features as dataset bias propagate into their neural network, which suffer from degraded performance in occluded or low-illuminated areas [22]. This is solved by modeling the uncertainty in a covariance model [23, 24]. Another improvement on traditional methods is the shift towards semantic VO. These methods use classifiers to stop features from being planted on dynamic objects, preventing false movement of features [25, 26]. Especially interesting for our planetary scenario, is the work by Liu et al. on learning-based feature matching in bland terrain where inaccurate feature (mis)matches cause critical localization errors. In the matching stage, they incorporate a retentive self-attention (RSA) module to enhance feature matching accuracy and local feature windows surrounding the key points are then fed into a transformer network to refine the feature point positions and filter out mismatches [27].

In contrast, **direct methods** bypass the explicit feature extraction and matching pipeline. Instead, they estimate motion by directly minimizing a photometric error, which is the sum of squared intensity differences of pixel patches between frames [28]. These methods leverage all photometric information, making them more robust in texture-poor environments where distinct features are scarce. Hybrid and semi-direct approaches also exist, combining the robustness of features at the keyframe level with the density of direct methods for frame-to-frame tracking [29]. Unfortunately, this does not guarantee robust performance in featureless terrain such as on Mars, as distinct pixel patches are also scarce at the crash site of Ingenuity.

Filtering vs. Optimization Once a relative motion estimate is obtained, it is integrated to refine the trajectory and mitigate the accumulation of drift. This is done using either filtering or non-linear optimization. **Filtering-based methods**, most notably those employing an Extended Kalman Filter (EKF), recursively update the system's state variables and their associated uncertainty. While computationally efficient and suitable for resource-constrained platforms, filters can suffer from accuracy degradation due to linearization errors and the inability to optimize past states [17, 29]. **Optimization-based methods** typically offer higher accuracy by formulating the estimation problem as a non-linear least-squares problem. These techniques jointly refine a set of variables—such as a window of the most recent sensor data—by minimizing the total re-projection error. This process is commonly referred to as Bundle Adjustment (BA). Although more computationally demanding than filtering, these methods are gener-

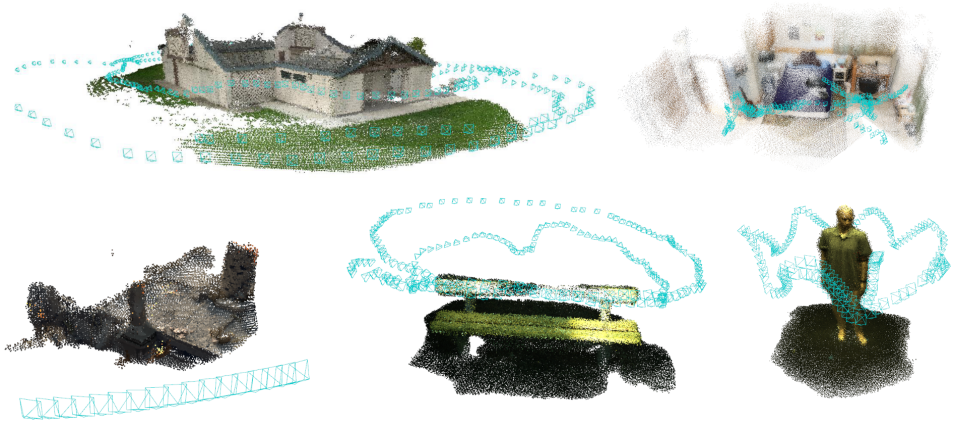

Figure 2.2: Point cloud map generated by DROID-SLAM from common evaluation datasets [23].

ally more accurate as they can incorporate information from multiple past frames and re-linearize the problem to find a more globally consistent solution [18, 19, 30, 28]. Recent advancement show the shift to learning-based methods. A major development in this area is Dense Bundle Adjustment (DBA). This DBA layer is implemented as a differentiable module that computes a Gauss-Newton update to jointly refine all camera poses and dense per-pixel depth maps in a single, global optimization problem across an arbitrary number of frames [23].

Sensor Suite The capabilities and robustness of a vision-based system are also defined by its sensor suite and its ability to correct for long-term drift. A simple system may use a single monocular camera, which is lightweight and simple but suffers from an inherent scale ambiguity—the absolute size of the environment and the trajectory cannot be determined without external information [31, 32, 33]. This ambiguity can be resolved by using a stereo camera pair, which provides a known baseline for depth triangulation, or an RGB-D sensor that directly supplies depth measurements [34, 30]. The fusion of visual data with an IMU is a common strategy, leading to VIO [17, 19, 30]. The high-frequency measurements from an IMU improve robustness to fast motions and in visually degraded environments, while also providing metric scale information. Beyond conventional cameras, specialized modalities enhance robustness for UAV operation. Event-based camera sensors asynchronously report pixel brightness changes, offering high temporal resolution, resilience to motion blur and under or over exposing, critical for fast-moving UAVs [35]. Thermal/infrared cameras provide complementary data for low-light or smoke-filled environments where visible spectrum information is insufficient [36].

Odometry vs SLAM While odometry systems focus on estimating local, incremental motion, they are susceptible to unbounded drift over long trajectories. To address this, odometry is often extended into Simultaneous Localization and Mapping (SLAM), which produces maps like pictured in Figure 2.2. The defining feature of SLAM is loop closure, the process of recognizing a previously visited location. Upon detection of a loop closure, a geometric constraint is added to the optimization, allowing the system to correct the accumulated drift across the entire trajectory and produce a globally consistent map and position estimate [30, 19]. Methods typically use techniques such as Bag-of-Words (BoW) using visual features in traditional methods or leverage deep learning to generate global image descriptors that are invariant to illumination or dynamic object changes, increasing accuracy of loop closures [23, 37].

Mapping with NeRF A state-of-the-art technique for dense 3D reconstruction involves representing the environment using a Neural Radiance Field (NeRF). This method models volume density and color by querying a neural network, enabling photorealistic reconstruction and offering a highly accurate, continuous map representation. Recent research has adapted these concepts for real-time localization, demonstrating the potential for dense, drift-free tracking within the generated implicit map [38, 39, 40]. Although still costly to run, these algorithms promise more accurate loop closure due to photo realistic representation, fill unobserved space plausibly and can represent spaces using small datasets [41].

Pruning Despite advancements in accuracy and efficiency, VIO systems remain computationally expensive. The image processing pipelines, particularly those using neural networks, impose a significant computational burden compared to the lightweight processing required for GNSS. This presents a challenge for UAV applications, as onboard computational power and energy are limited—a constraint often referred to as SWaP. This is even more challenging considering the need for high-frequency state estimates, which are critical for maintaining stable flight control during rapid maneuvers.

To bridge this gap, a key research section is the development of specialized, lightweight algorithms for resource-constrained platforms. This often involves pruning more complex systems to reduce their computational load while preserving localization accuracy. For instance, Kuhne et al. [42] demonstrate this by integrating ORB and SuperPoint features on a microcontroller for 2.5D visual odometry. Wang et al. [43] introduce a lightweight positioning network that uses a trimmed-down YOLOv8n model to filter out dynamic objects, improving robustness.

Conclusion There is a clear trend away from purely geometric, feature-based methods toward more sophisticated systems that leverage deep learning and implicit neural representations like NeRFs. However, this progress introduces a critical trade-off, as the transition to learning-based architectures increases the computational demand. While techniques such as Dense Bundle Adjustment and NeRF-based mapping offer better performance, their computational and memory requirements are often prohibitive for the limited SWaP budgets of most UAV platforms.

Besides computational load, other challenges still face VO algorithms. Drift accumulation is an issue that causes a gradual error between the ground truth and the estimated position. This is caused by the VO algorithm integrating small motion estimation errors over time. While SLAM frameworks address this through loop closure, increasing the computational burden, the reliable detection and correction of drift over long-duration flights, especially in perceptually ambiguous or dynamic environments, remains an open research problem. Performance in visually degraded scenarios, such as texture-poor terrain, adverse lighting conditions, or environments with significant motion blur, also continues to be a primary failure point. Although learning-based feature extractors and direct methods have improved resilience, no single solution has emerged that guarantees robust operation across all conditions, as is needed for planetary exploration.

Table 2.1 provides a classification of several influential VIO and SLAM algorithms based on these design principles. Besides sensor requirements, the need for rich features, refresh rate and computational power is especially interesting for our scenario. It can be seen that many methods require rich features and run at relatively low refresh rates, which indicates low robustness when moving fast through featureless terrain. The computational platforms that these algorithms are validated on can also be a cause for concern, as almost all algorithms are evaluated on premium desktop hardware.

2.3. Other Sensors

Besides visual and inertial sensors, other sensors can be used in the context of odometry and localization. As previously mentioned, cameras still suffer from fundamental issues, like over/under-exposure, low temporal resolution, vulnerabilities caused by textureless terrain and high bandwidth requirements. Other sensors can aid or provide localization where cameras fall short.

LiDAR Scanning its surroundings, LiDAR delivers accurate, long-range 3D geometry independent of lighting conditions. Spinning or solid-state LiDAR sensors can build high-resolution 360 point clouds of their surroundings with centimeter accuracy over long ranges without noticable drift [52]. Traditional SLAM methods use the Iterative Closest Point (ICP) algorithm, where an initial estimate is made based on inertial or wheel odometry. Then dynamic points are filtered out to capture solid reference objects, after which the point cloud is iteratively moved, slowly minimizing the distance between each point of the point cloud [53]. Instead of this point-to-point method, modern frameworks use point-to-plane, where n nearest points are taken for each new point, representing a plane. Using the normal vector between this plane and the new point, the new point cloud is moved in position to minimize this error vector for each new point [52]. This method has shown faster convergence and higher accuracy than traditional methods. Using these methods, LiDAR can provide an accurate first estimate and depth

Table 2.1: Comprehensive classification of influential SLAM and odometry algorithms, detailing their tracking methodology, backend, supported sensor suites, need for features, performance and compute requirements, where I is Intel and N is NVIDIA.

Algorithm	Year	Tracking	Refinement	LC	Mono	Stereo	RGB-D	IMU	Feat.	Hz	Compute
MSCKF [17]	2007	Features	Filtering		✓	✓		✓	✓	14	I T7200
MonoSLAM [31]	2007	Features	Filtering		✓				✓	30	I Pentium M
PTAM [32]	2007	Features	Optimization		✓				✓	30	I Core 2 Duo
DTAM [33]	2011	Direct	Optimization		✓					30	N GTX 480
KinectFusion [34]	2011	Direct	Volumetric Fusion				✓			10	N/A
DVO-SLAM [44]	2013	Direct	Optimization	✓			✓			31	I Core i7-2600
SLAM++ [45]	2013	Hybrid	Optimization	✓			✓		✓	20	Gaming laptop
LSD-SLAM [46]	2014	Direct	Optimization	✓	✓					30	N/A
OKVIS [18]	2014	Features	Optimization		✓	✓		✓	✓	20	N/A
RGBDSLAMv2 [47]	2014	Features	Optimization	✓			✓		✓	30	N GTX 570
SVO [48]	2014	Hybrid	Optimization		✓	✓		✓	✓	50	Odroid U2
ROVIO [29]	2015	Hybrid	Filtering		✓			✓		20	I i7-2760QM
CNN-SLAM [49]	2017	Direct	Optimization	✓	✓					N/A	N Q K5200
ORB-SLAM2 [50]	2017	Features	Optimization	✓	✓	✓	✓		✓	N/A	I i7-4790
VIORB [51]	2017	Features	Optimization	✓	✓			✓	✓	20	I i7-4700MQ
VINS-Mono [19]	2018	Features	Optimization	✓	✓	✓		✓	✓	25	I i7-4790
Kimera [25]	2020	Semantic/Features	Optimization	✓		✓	✓	✓	✓	18	N/A
D3VO [22]	2020	Direct/Learning	Optimization		✓			✓		20	N/A
ORB-SLAM3 [30]	2020	Features	Optimization	✓	✓	✓	✓	✓	✓	20	I i7-7700
DROID-SLAM [23]	2021	Learning	Learning (DBA)	✓	✓	✓	✓		✓	20	2x N RTX 3090
YOLO-SLAM [26]	2022	Semantic/Features	Optimization	✓	✓	✓	✓		✓	1.5	I i5-4288U
NICE-SLAM [39]	2022	Direct/Learning	NeRF Mapping	✓	✓		✓			20	N RTX 3090
NeRF-SLAM [38]	2023	Direct/Learning	NeRF Mapping	✓	✓					20	N RTX 2080Ti
MAC-VO [24]	2025	Features/Learning	Learning (DBA)		✓				✓	10	N RTX 3090
SP-SLAM [40]	2025	Direct/Learning	NeRF Mapping	✓	✓					12	N RTX 3090Ti
RISC-VO [42]	2025	Features	Filtering		✓			✓	✓	120	GAP9
MAR-VO [27]	2025	Features/Learning	Learning		✓				✓	15	N RTX 4070

data for VIO, while still leveraging semantics and texture richness of cameras. This adds another layer of safety against critical failures and enables stable SLAM.

Although LiDAR is a solid data source, their impact on a UAV's SWaP budget –which is critical in extraterrestrial missions– are quite large. Depending on the specific sensor, the power consumption is high, varying from 8 to 15 W [54] and can be heavy on smaller drones compared to cameras. Besides physical limitations, performance degrades in rain or fog or with transparent/specular objects, and the data are sparse at a distance [55, 56], which means using LiDAR as the only perception source is not viable yet, especially in planetary exploration.

Radar In adverse weather or smoky environments, LiDAR and cameras stops working as light is blocked by small particles, as can be seen in Figure 2.3. This is where radar shines, as longer radio waves are not affected by rain and fog, offering range and Doppler velocity perception [57]. This is also a reason why radar is popular in the car industry, as collision prevention and adaptive cruise control methods need a stable and robust measurement of their surroundings. However, radar systems provide limited resolution and often offer sparse 2D point clouds and lower angular accuracy compared to LiDAR [57]. This sparsity, combined with significant noise makes the extraction of precise geometric features challenging, thus complicating standalone localization.

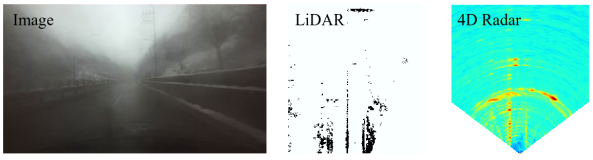

Figure 2.3: Comparison of a snapshot of a camera, LiDAR and Radar system [57].

Recent advancements, particularly the development of 4D imaging radar, have begun to address these shortcomings. By providing an additional elevation dimension alongside range, azimuth, and Doppler velocity, 4D radar enables the generation of denser, 3D point clouds that are more suitable for localization and mapping tasks, although expensive [57].

Another method used for precise localization is Ultra Wideband (UWB). UWB systems leverage high-bandwidth pulses to achieve centimeter-level accuracy. These systems are particularly effective for indoor navigation, especially smoky or low-visibility environments, but do require UWB infrastructure installed. Tiemann et al. [58] show how a UWB localization system can be augmented with monocular SLAM to enable a UAV to navigate in areas not covered by the UWB infrastructure, switching between

UWB and VO. Premachandra et al. [59] uses UWB to locate walls and landmarks in foggy environments, using wheel odometry as main localization, combined with an UWB loop closure mechanism.

Sensors like LiDAR, Radar, and UWB offer advantages in specific scenarios, but each possess limitations that prevent them from being used as standalone localization solutions for a drone, especially in the context of Martian exploration. LiDAR imposes a significant burden on the drone's SWaP budget, despite its high accuracy. Radar offers robustness in bad weather but has degraded resolution and data sparsity compared to visual methods, making it difficult to build the detailed environmental maps necessary for precise localization. At last, UWB is impractical for planetary exploration as it relies on pre-deployed infrastructure, which is hard to realize on Mars. Therefore, these sensors are best utilized within a sensor fusion framework where they can augment vision-based systems, rather than replace them entirely.

2.4. Conclusion

In this chapter, we examined current approaches to UAV localization and their vulnerabilities in a planetary exploration scenario. GNSS-based localization proves to be accurate on Earth with sub-cm scale, especially with RTK and PPP methods, but is unfortunately not available on Mars. This leaves us with infrastructure-agnostic methods.

VO and other vision-based methods depend on visual features for motion estimation. As these methods are crucial in the field of robotics, lots of algorithms are proposed each year, from simple geometric feature detectors to learning-based self-attention modules for bland terrain feature extracting. These visual features are critical for smooth operation, as textureless terrain can cause vital problems, independent of how advanced the feature extractor gets. This was demonstrated in the case of Ingenuity, which crashed into a bland and featureless sand dune on Mars. Aside from featureless terrain, small SWaP budgets, which are crucial on space missions, also restrict the compute on drones, introducing another constraint for complex learning-based VO algorithms that can be used to compensate for bland terrain and limited sensors. Besides the lack of features, VO and other integrating methods suffer from drift accumulation. These can be compensated for with expensive SLAM algorithms or GNSS fusion, but both are not viable in planetary exploration settings.

To fix these problems with vision-based methods, LiDAR and radar can be used to increase visual perception through 3D scans. Unfortunately, these sensors are not suitable to fly on a Martian drone due to their impact on the SWaP budget, especially as they are not yet suited for standalone localization.

In summary, conventional localization methods still suffer from crucial limitations that become especially visible in a Martian setting, such as feature-sparse terrain, drift accumulation, small SWaP budgets and inadequate backup methods. Ingenuity, although a success story, serves as a reminder that these limitations are real and need to be mitigated. This establishes a clear need for alternative localization methods that can operate in Martian exploration scenarios.

3

Tether State Position Estimation

In this chapter, we will review existing methods that use state variables of a tether between a TUAV and base robot pair for localization of the TUAV, analyzing their robustness and accuracy. Although a niche topic, numerous works have investigated the feasibility of using this tether to enhance or provide localization relative to the base robot. The nature of this position estimation method seems promising, as a small amount of variables can be used to derive the tether state from relatively simple geometric equations. This allows us to free up SWaP budget as there is no high demand for compute, compared to more expensive methods discussed in the previous chapter.

3.1. Taut-Tether Methods

Rudimentary methods constrain themselves to the taut-tether paradigm, meaning that the tether is modeled as a straight line. Besides the simple trigonometric nature of this method, less sensor data is needed as only the bases length, azimuth and elevation angle is required for calculating the end position of a tether, as can be seen in Figure 3.1a. A downside of this approach is that the tether needs to be in increasingly higher tension as tether length increases to keep it taut, adding additional forces to the UAV. However, this can also benefit the stability of a landing UAV [61]. Furthermore, the taut tether model is resilient to fast maneuvers, as oscillatory behavior of the tether is limited [62].

Alarcón et al. [63] propose this method to land a UAV helicopter on a 3D moving platform, to simulate landing on a ship. The helicopter hooks to a moving platform using a tether, where the drone's tether angle is sensed by an angle sensor attached to a loadcell for tension measurements. This tension is controlled at a setpoint of approximately $20\,\mathrm{N}$ and excess tether is spooled on the moving platform.

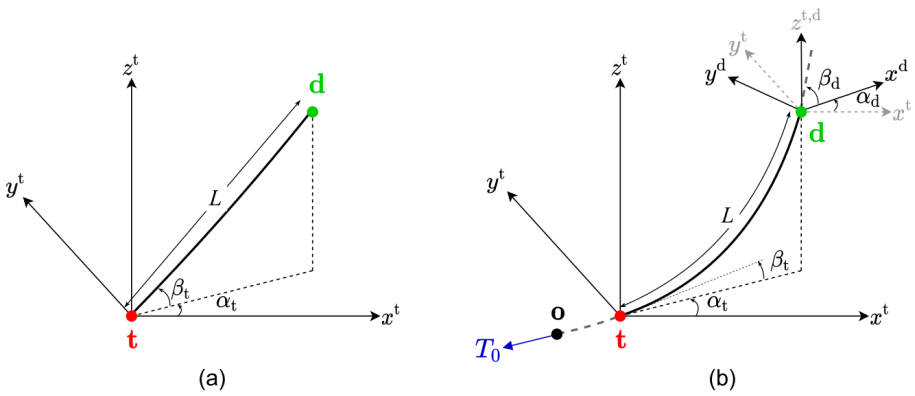

Figure 3.1: The difference between a taut and a catenary tether model, where (a) represents the taut model and (b) represents a catenary model (Taken from [60]). It can be seen that a taut model needs less sensing than a catenary model, as the tension T_0 and drone elevation angle β_d is required for the pictured catenary model.

They use the initial tether position estimate in an EKF, fusing IMU and tether properties. Using RTK-GNSS as ground truth to verify the position estimate, a RMSE of $0.20\,\mathrm{m}$ is determined. This is deemed sufficient as the landing platform is $3\,\mathrm{m}$ wide. Error sources include helicopter ground effect which causes a large spike in tension as the helicopter nears the platform and angle sensor inaccuracies, as plots show constant deviations in horizontal position.

Al-Radaideh et al. [64] use a taut tether model in combination of a tether angle estimation algorithm. This algorithm uses Pulse Width Modulation (PWM) motor values to calculate the thrust vector of the drone, which is used in combination with the onboard IMU to calculate the direction of the attached tether. The tether vector, combined with the length of the tether, which is assumed to be in constant tension, is then merged in an EKF. The motivation behind this method is that no additional sensors are required for the localization of a tethered drone, only the cable length, which is often trivial to retrieve in a commercial Tether Management System (TMS). Verification of their model happens in simulation, resulting in a minimum RMSE of $0.18\,\mathrm{m}$, given a constant tension of $4\,\mathrm{N}$. Various other scenarios are tested, with heights from $1\,\mathrm{m}$ to $10\,\mathrm{m}$, velocities of $0.5\,\mathrm{m/s}$ to $3\,\mathrm{m/s}$ and tension from $0.5\,\mathrm{N}$ to $10\,\mathrm{N}$. They motivate their choice for a taut model because of the dynamic use case, but show a clear increase of error with higher drone velocities. Unfortunately no testing was done on a real test platform. As the proposed methods relies heavily on sensors that typically are subjected to noise, the feasibility for physical systems remains unverified.

As mentioned above, the biggest downside of the taut model is that the tether needs to be in high tension (up to $20\,\mathrm{N}$), increasing the required energy to stay in flight, which comes back to our limited SWaP budget. This is not that important for a scenario on Earth, as power could be delivered via the cable from the ground. Unfortunately, our rover is limited in its power generation, making this method not suitable for our scenario.

3.2. Flexible Tether Methods

More advanced methods account for the slacking tether as it gets longer, which is modeled as a catenary. This catenary requires more constraining variables, and thus more sensors, but allows for minimum tension in the tether. The catenary model works under the assumption of a quasi-static state, meaning that the cable is only affected by the two endpoint forces and a uniform gravitational field [65]. This means any oscillatory behaviour of the tether, dynamic maneuvers and wind can impact the accuracy of the position estimate.

Kiribayashi et al. [66] propose a catenary model where the tether position is calculated by measuring tether length, tension and outlet direction using a custom built sensor suite at the base station. The tension vector, which is derived from the base angle sensor (as seen in Figure 3.2a) and tension sensor, is used in an force equilibrium calculation together with the tether weight to determine the UAV position.

$$z = a\cosh\left(\frac{x}{a}\right) - a, \quad a = \frac{T_0}{\rho g} \tag{3.1}$$

where T_0 is the tension in the vertex, ρ the tether density and g the gravitational coefficient.

An indoor flight experiment, that uses motion capture as ground truth, show errors of $1.0\,\mathrm{m}$ for diagonal motion at $5.0\,\mathrm{m}$ tether length. It is theorized that this error is caused by error in the angle sensor, error in the tension controllable winch and/or stiffness or twists in the tether, causing a discrepancy between the catenary model and the real world scenario. As there is an angular offset in the flightpath plot, originating from the TMS, it is likely that the angle sensor is at fault.

Xiao et al. [67] propose a method that employs a commercial TMS that measures length and direction at the TMS. The tension is derived from the weight of the drone and the amount of dispensed cable, together with the UAV attitude relative to the horizontal plane. The catenary coefficient is then calculated similar to the method of Kiribayashi et al. [66], which is used in an equation that determines the difference between the tether and straight line elevation angle. This difference is then added to the tether elevation angle, leaving us with the proper elevation angle of the drone. The same compensation is done for the tether length, which gives us the position of the drone in spherical coordinates, which then needs to be converted to cartesian coordinates. Indoor experimental validation with motion capture ground truth achieved $0.37\,\mathrm{m}$ average error at maximum tether lengths of $3.25\,\mathrm{m}$. Compared

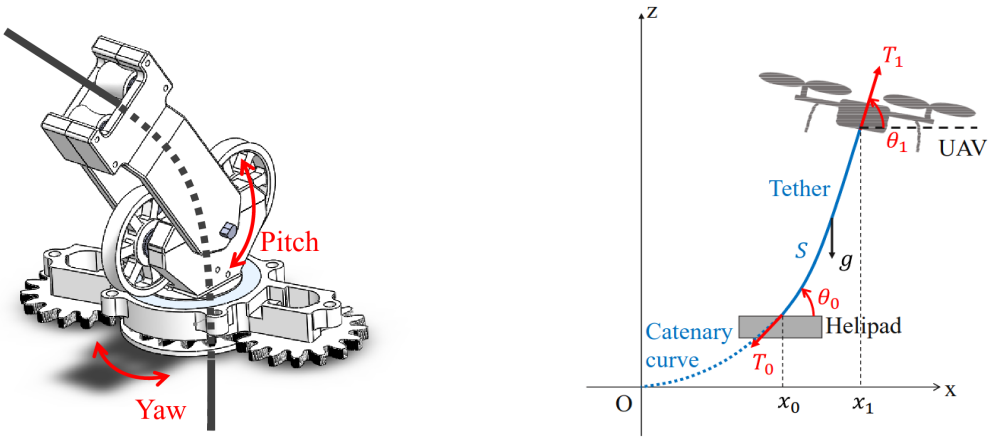

(a) Design of a sensor that reads the departure angle at the base of the TMS, while passing the tether to the tether spool [66].

(b) Free Body Diagram of the UAV with the force equilibrium of the tension and gravity forces [66].

Figure 3.2: Supporting figures of Kiriayashi et al. [66].

to previous methods, the steps towards the position estimate seem quite convoluted, as the cartesian position could also be derived from the catenary equation, instead of compensating the sensed tether angle. Secondly, the tension acquisition strategy seems flawed, as tension is inferred from the weight of the drone and tether, neglecting any dynamic effects or motor perturbations.

Borgese et al. [68] use custom hardware mounted on a rover which measures angles at both ends of the tether, but uses a fixed length tether, making a TMS obsolete. The tether position model uses the same catenary equations as Kiribayashi et al. [66] and Xiao et al. [67], except that the catenary coefficient a is calculated using the arc length and tether angles, instead of using the tether tension. The method is tested with a few static flightpoints and two outdoor flight tests, consisting of 5 or 8 waypoints, using RTK-GNSS as a ground truth and position feedback. They are able to achieve an average error of $0.66\,\mathrm{m}$ at a tether length of about $5\,\mathrm{m}$. It is stated that some error was caused by friction in the azimuth direction of the base angle sensor, although this does not explain the big radial offset between the ground truth and position estimates throughout all experiments. The negative offset suggests a problem with the elevation angle sensors or the drone attitude compensation of these angles.

Most recently, Lima et al. [60] propose a trained classifier that chooses from three different models, a trigonometric (taut), a catenary and a neural network model according to the current state variables (angles, length, tension). These tether state variables gathered using custom built length, tension and UAV and base angle sensors. Besides selecting the best model, the selector also tries to detect when tether localization is not possible, e.g. when the tether is touching the ground, sensors are saturated or the drone flies too low. The selectors are trained on a dataset consisting of 31 k samples, collected during indoor (motion capture ground truth) and outdoor flights (GNSS ground truth). For every sample, the model with the lowest absolute error is picked, with a maximum error of $0.45\,\mathrm{m}$. If none of the models reach this accuracy, the selector is trained to output that no localization is possible. The framework is evaluated on more indoor and outdoor flight data, where the RMSE from the catenary model is $1.27\,\mathrm{m}$ and the complete framework reports a RMSE of $1.1\,\mathrm{m}$. The poor performance is stated to be due to bad selector training, as the GNSS ground truth data is inaccurate and indoor test flights are limited in height. Besides poor selection performance, the catenary model also shows high error values, which is explained by the paper as caused by the stiffness of the tether.

From these works it can be derived that a catenary model can be used as a way to predict the position of the drone at the end of a slacking tether, but hard to get the accuracy to a workable range. As most experiments are conducted on custom hardware, error sources can be hard to pinpoint. While the latest research tries to bridge this gap with learning-based methods for position estimation, reported errors are still too high to use reliably in a drone's control loop.

Table 3.1: Summary of Tether State Estimation Localization Methods, where L is length, T is tension, $\angle_b$ is base angle and $\angle_d$ is drone angle.

Method	Error (m)	L (m)	Sensors	Catenary/Taut	Environment	Ground Truth
[63]	0.23	10	$\angle_d$, L, IMU	T	Outdoor	RTK-GNSS
[64]	0.30	10	IMU, Motor PWM	T	Simulation	Simulation
[66]	1.0	5	$\angle_b$, L, T	C	In & outdoor	Mo-cap
[67]	0.37	3.3	$\angle_b$, L, IMU	C & T	Indoor	Mo-cap
[68]	0.66	5	$\angle_b$, $\angle_d$	C	Outdoor	RTK-GNSS
[60]	1.1	6	$\angle_b$, $\angle_d$, L, T	C & T	In & outdoor	Mo-cap

3.3. Conclusion

Tether-based localization shows that positioning can be achieved with relatively simple algorithms and sensors. Besides Lima et al. [60], all methods only used a couple of analytical mathematical equations, meaning localization can be done on a low power micro controller. While tether-based localization is a promising technique, it can be seen that taut tether models and catenary models still have their downsides. Taut tether methods are more accurate, given that the tether is kept in tension. However, as tether lengths increase, this assumption begins to degrade and becomes an unacceptable burden on the drones payload. The catenary models slacking tethers, freeing up SWaP budget in return for more sensing. A clear gap then becomes apparent, as errors in the catenary regime are too large for precise flight control, which can be seen in Table 3.1. This highlights the need for a framework that is both physically principled, thus using a catenary model, and capable of compensating for subtle real-world non-linearities in real-time.

4

Discussion & Conclusion

This work has aimed to answer two important questions by evaluating the research question; *"To what extent can tether-based localization systems for UAVs mitigate the performance limitations of conventional UAV pose estimation in the context of planetary exploration?"*

4.1. Discussion

To answer this research question, this work first looks at the limitations of conventional UAV localization. GNSS localization seems to be the general default with autonomous drones, sometimes supported by RTK or PPP technology, as this provides a cheap and reliable position estimate. This method begins to break down when satellites disappear from visibility, either by tall buildings or when moving indoors or into space. Most UAVs then switch to VO or similar vision-based technologies. Using complex algorithms, the drone is able to keep track of their relative position w.r.t. the starting point. The main issues of these odometry-type methods are position drift, as small errors grow bigger, processing, as compute impacts the SWaP budget and loss of reference features, when the environment turns bland. These last two issues are amplified in a Martian scenario, as SWaP budgets are extremely tight and as Ingenuity VO system failed to detect features, causing an unrecoverable crash.

4.1.1. Tether Localization Tradeoffs

We then establish that an alternative localization technique is required. As tethering the drone to a rover would help SWaP issues, we investigate if this tether can also aid in localization. Two main tether localization paradigms exist, the taut or the slacking tether, modeled by a trigonometric or catenary equation, respectively. The trigonometric method is preferred in scenarios where power is not constrained and tether lengths will be short or vertical, as the TUAV will be able to keep the tether taut. The accuracy in the analyzed methods has a range of $0.23\,\mathrm{m}$ to $0.30\,\mathrm{m}$, which is a good starting point for further research. Another benefit of the taut paradigm is the limited sensor suite that is required, as only the tether length and the base or drone angle, which can also be derived from the drone's attitude, needs to be sensed. However, the energy needed to sustain a straight tether increases dramatically as the tether length grows, leading to an unacceptable burden on the UAV.

When switching to the catenary model, enabling us to model the tether sag, the main challenge becomes the reliable and accurate sensing of the tether state. Some methods try to infer the tether state from indirect sensing by inferring the tether angle with the drone's attitude, which can cause sensitivity to error in non-static scenarios due to the non-linear nature of this inference and model uncertainties. This seems to be an issue with current catenary works, as no accuracy better than $0.37\,\mathrm{m}$ is reported and limited verification data is available. The measurement of tether angles through dedicated sensors, which are also hard to fabricate and calibrate, provides more reliable data than through sensitive inference, but increases system complexity and potential failure modes.

In Table 4.1, these tradeoffs seen in current works are summarized. As we established before, low tension is needed in the resource constraint environment of Mars, meaning direct tether state mea-

Table 4.1: Primary trade-offs between state-of-the-art tether-based localization literature.

Trade-off	Option A	Option B
Taut vs. Catenary	*Trigonometric Model:* 2 dimensional sensing (length + single angle); achieves $0.23\,\mathrm{m}$ to $0.30\,\mathrm{m}$ error; requires high tension ($4\,\mathrm{N}$ to $20\,\mathrm{N}$)	*Catenary Model:* 4 dimensional sensing (length, tension, base and drone angles); achieves $0.23\,\mathrm{m}$ to $1.1\,\mathrm{m}$ error; operates at low tension
Direct vs. Indirect sensing	*Indirect Measurement:* Infers angles from IMU/thrust; minimal hardware; sensitive to dynamics and model errors	*Direct Measurement:* Dedicated angle sensors; increased hardware complexity; robust to dynamics but additional failure modes
Tension vs. Payload	*High Tension:* Enables taut model with simpler estimation; consumes power for tension maintenance; limits mission duration	*Low Tension:* Reduces power consumption; frees SWaP budget; requires catenary compensation with current accuracy penalties

surement is required.

4.1.2. Research Gaps

Several gaps prevent tether-based localization from achieving the accuracy required for precise flight control. As a catenary is proven to be an exact representation of a freely hanging tether [69], errors need to be sought for outside the theoretical model if all assumptions of the model are met. The reviewed works report high errors, but lack in-depth examination on how this error emerges. Multiple studies allot errors to inaccuracies in tether angle variables, which introduce noise and offsets in the estimated position. The use of indirect angle estimation from thrust vectors or attitude data appears to exacerbate this behavior. An error propagation analysis, using measured tether state variable uncertainties, could clarify which input variables have the largest impact on positioning accuracy.

The use of custom hardware in almost all reviewed works, besides a commercial TMS in the work of Xiao et al. [67], highlights a maturity gap in tethered systems. Future work could proof the viability of tether localization by proper sensor design, calibration and verification, as to eliminate sensor error one-by-one. A fully instrumented TMS could then be the testbed for further ablation studies of tether angles derived from UAV attitude, or other indirect measurement methods, while establishing a performance baseline of full tether state estimation. This method would give us more tools to approach the accuracy-complexity trade-off than current literature, paving the way for future commercialized systems. For these systems to commercialize, more fault tolerance research should be done. Tether-based systems face unique failure modes including sensor malfunction, tether entanglement, and model assumption violations. For systems to stay robust, failures must be detected and either compensated or gracefully degraded to other localization modes.

Building on top of this TMS, residual error compensation methods could further enhance accuracy. Besides merging IMU data, tether state and catenary position estimate into an EKF, which we have seen in previous works, we could try to compensate residual error, caused by inevitable sensor deviations. This residual error compensation could be performed by a learning-based method, where the algorithm learns the small offsets of the particular TMS and can compensate these during flight, eliminating any steady-state error.

4.2. Conclusion

This work has reviewed conventional and tether-based localization methods for UAVs in planetary exploration contexts, such as Mars. The primary limitations of conventional methods in GNSS-denied environments are:

- Unbounded drift accumulation in odometry-based systems.

- Feature dependent vision-based localization that fails in bland terrain.
- Computational costs that conflict with SWaP constraints.
- Lack of absolute position corrections without other infrastructure.

These limitations create a need for alternative positioning methods.

To combat other issues like limited SWaP budget and rover visibility, a tethered UAV rover team is proposed. Exploiting this tethered system, tether-based localization addresses these conventional positioning constraints by providing drift-free relative localization with minimal computational requirements. Taut-tether approaches achieve $0.23\,\mathrm{m}$ to $0.3\,\mathrm{m}$ accuracy but impose high tension requirements ($4\,\mathrm{N}$ to $20\,\mathrm{N}$) that scale poorly as length increases, making them unsuitable for planetary missions with limited SWaP budgets. Catenary-based methods accommodate longer tethers with reduced tension but currently fair poorly in terms of accuracy ($0.37\,\mathrm{m}$ to $1.1\,\mathrm{m}$), which is too unreliable for autonomous. However, these errors are mainly caused by sensor inaccuracies and indirect measurement approaches rather than model limitations.

To answer the main research question: tether-based localization systems are promising for mitigating the performance limitations of conventional localization in planetary exploration, especially regarding computational efficiency and drift-free environment agnostic operation. However, state-of-the-art implementations of this technology do not yet achieve the accuracy required for reliable drone control. The best way forward includes improving sensor quality and developing residual error compensation algorithms in catenary-based systems.

Future work should prioritize:

- Error propagation analysis to pinpoint error sources.
- Development of reliable, accurate and fully instrumented test platforms.
- Residual error compensation using learning-based methods.
- Validation at larger tether lengths and environmental conditions, analyzing failure modes.

These steps should mature tether-based localization to reach the reliability for planetary exploration missions.

References

[1] Nicolas Mangold et al. “Perseverance rover reveals an ancient delta-lake system and flood deposits at Jezero crater, Mars”. In: *Science* 374.6568 (2021). Publisher: American Association for the Advancement of Science, pp. 711–717.

[2] J Balaram, MiMi Aung, and Matthew P Golombek. “The ingenuity helicopter on the perseverance rover”. In: *Space Science Reviews* 217.4 (2021). Publisher: Springer, p. 56.

[3] D. C. Agle. Publication Title: NASA. 2024. URL: https://www.jpl.nasa.gov/news/nasa-performs-first-aircraft-accident-investigation-on-another-world/.

[4] Mohamed Nadir Boukoberine, Zhibin Zhou, and Mohamed Benbouzid. “Power supply architectures for drones-a review”. In: *IECON 2019-45th Annual Conference of the IEEE Industrial Electronics Society*. Vol. 1. IEEE. 2019, pp. 5826–5831.

[5] Naser Hossein Motlagh, Miloud Bagaa, and Tarik Taleb. “UAV-based IoT platform: A crowd surveillance use case”. In: *IEEE Communications Magazine* 55.2 (2017), pp. 128–134.

[6] Reza S. Omandam et al. “3D Localization of Suspended and Tethered Drone for High-rise Bridge Inspection”. In: *2022 IEEE 14th International Conference on Humanoid, Nanotechnology, Information Technology, Communication and Control, Environment, and Management (HNICEM)*. 2022, pp. 1–6.

[7] Bernardo Martinez Rocamora et al. “Oxpecker: A Tethered UAV for Inspection of Stone-Mine Pillars”. In: *Drones* 7.2 (2023). ISSN: 2504-446X.

[8] Alpaslan Durmus, Erol Duymaz, and Mehmet Baran. “The Use of Tethered Unmanned Aerial Vehicles in the Field of Defense and Current Developments”. In: *New Technologies and Developments in Unmanned Systems*. Ed. by T. Hikmet Karakoc et al. Cham: Springer International Publishing, 2023, pp. 207–214. ISBN: 978-3-031-37160-8.

[9] C. Rizos. “Network RTK Research and Implementation: A Geodetic Perspective”. In: *Journal of Global Positioning Systems* 1.2 (Dec. 2002), pp. 144–150. ISSN: 14463156, 14463164. DOI: 10.5081/jgps.1.2.144. URL: http://www.gnss.com.au/JoGPS/v1n2/v1n2pI.pdf (visited on 09/24/2025).

[10] Marco Pini et al. “Experimental Testbed and Methodology for the Assessment of RTK GNSS Receivers Used in Precision Agriculture”. In: *IEEE Access* 8 (2020), pp. 14690–14703. ISSN: 2169-3536. DOI: 10.1109/ACCESS.2020.2965741. URL: https://ieeexplore.ieee.org/abstract/document/8955794 (visited on 09/24/2025).

[11] Guanwen Huang, Shi Du, and Duo Wang. “GNSS techniques for real-time monitoring of landslides: a review”. en. In: *Satellite Navigation* 4.1 (Feb. 2023), p. 5. ISSN: 2662-1363. DOI: 10.1186/s43020-023-00095-5. URL: https://doi.org/10.1186/s43020-023-00095-5 (visited on 09/24/2025).

[12] J. F. Zumberge et al. “Precise point positioning for the efficient and robust analysis of GPS data from large networks”. en. In: *Journal of Geophysical Research: Solid Earth* 102.B3 (1997). _eprint: https://agupubs.onlinelibrary.wiley.com/doi/pdf/10.1029/96JB03860, pp. 5005–5017. ISSN: 2156-2202. DOI: 10.1029/96JB03860. URL: https://onlinelibrary.wiley.com/doi/abs/10.1029/96JB03860 (visited on 09/24/2025).

[13] Jianghui Geng et al. “Inter-system PPP ambiguity resolution between GPS and BeiDou for rapid initialization”. en. In: *Journal of Geodesy* 93.3 (Mar. 2019), pp. 383–398. ISSN: 1432-1394. DOI: 10.1007/s00190-018-1167-6. URL: https://doi.org/10.1007/s00190-018-1167-6 (visited on 09/24/2025).

[14] C. Chi et al. “Enabling robust and accurate navigation for UAVs using real-time GNSS precise point positioning and IMU integration”. en. In: *The Aeronautical Journal* 125.1283 (Jan. 2021), pp. 87–108. ISSN: 0001-9240, 2059-6464. DOI: 10.1017/aer.2020.80. URL: https://www.cambridge.org/core/product/identifier/S0001924020000809/type/journal_article (visited on 09/24/2025).

[15] Feng Wang and Jianghui Geng. “GNSS PPP-RTK tightly coupled with low-cost visual-inertial odometry aiming at urban canyons”. en. In: *Journal of Geodesy* 97.7 (July 2023), p. 66. ISSN: 0949-7714, 1432-1394. DOI: 10.1007/s00190-023-01749-7. URL: https://link.springer.com/10.1007/s00190-023-01749-7 (visited on 09/24/2025).

[16] Joel J.K. Parker et al. “The Lunar GNSS Receiver Experiment (LuGRE)”. en. In: Long Beach, California, Feb. 2022, pp. 420–437. DOI: 10.33012/2022.18199. URL: https://www.ion.org/publications/abstract.cfm?articleID=18199 (visited on 10/13/2025).

[17] Anastasios I. Mourikis and Stergios I. Roumeliotis. “A Multi-State Constraint Kalman Filter for Vision-aided Inertial Navigation”. In: *Proceedings 2007 IEEE International Conference on Robotics and Automation*. ISSN: 1050-4729. Apr. 2007, pp. 3565–3572. DOI: 10.1109/ROBOT.2007.364024. URL: https://ieeexplore.ieee.org/abstract/document/4209642 (visited on 09/25/2025).

[18] Stefan Leutenegger et al. “Keyframe-based visual–inertial odometry using nonlinear optimization”. EN. In: *The International Journal of Robotics Research* 34.3 (Mar. 2015). Publisher: SAGE Publications Ltd STM, pp. 314–334. ISSN: 0278-3649. DOI: 10.1177/0278364914554813. URL: https://doi.org/10.1177/0278364914554813 (visited on 09/25/2025).

[19] Tong Qin, Peiliang Li, and Shaojie Shen. “VINS-Mono: A Robust and Versatile Monocular Visual-Inertial State Estimator”. In: *IEEE Transactions on Robotics* 34.4 (Aug. 2018), pp. 1004–1020. ISSN: 1941-0468. DOI: 10.1109/TRO.2018.2853729. URL: https://ieeexplore.ieee.org/abstract/document/8421746 (visited on 09/25/2025).

[20] Daniel DeTone, Tomasz Malisiewicz, and Andrew Rabinovich. *SuperPoint: Self-Supervised Interest Point Detection and Description*. arXiv:1712.07629 [cs] version: 4. Apr. 2018. DOI: 10.48550/arXiv.1712.07629. URL: http://arxiv.org/abs/1712.07629 (visited on 09/29/2025).

[21] Philipp Lindenberger et al. *Pixel-Perfect Structure-from-Motion with Featuremetric Refinement*. arXiv:2108.08291 [cs]. Aug. 2021. DOI: 10.48550/arXiv.2108.08291. URL: http://arxiv.org/abs/2108.08291 (visited on 09/29/2025).

[22] Nan Yang et al. *D3VO: Deep Depth, Deep Pose and Deep Uncertainty for Monocular Visual Odometry*. arXiv:2003.01060 [cs]. Mar. 2020. DOI: 10.48550/arXiv.2003.01060. URL: http://arxiv.org/abs/2003.01060 (visited on 09/29/2025).

[23] Zachary Teed and Jia Deng. “DROID-SLAM: Deep Visual SLAM for Monocular, Stereo, and RGB-D Cameras”. In: *Advances in Neural Information Processing Systems*. Vol. 34. Curran Associates, Inc., 2021, pp. 16558–16569. URL: https://proceedings.neurips.cc/paper/2021/hash/89fcd07f20b6785b92134bd6c1d0fa42-Abstract.html (visited on 09/29/2025).

[24] Yuheng Qiu et al. *MAC-VO: Metrics-aware Covariance for Learning-based Stereo Visual Odometry*. arXiv:2409.09479 [cs]. Mar. 2025. DOI: 10.48550/arXiv.2409.09479. URL: http://arxiv.org/abs/2409.09479 (visited on 09/29/2025).

[25] Antoni Rosinol et al. *Kimera: an Open-Source Library for Real-Time Metric-Semantic Localization and Mapping*. arXiv:1910.02490 [cs]. Mar. 2020. DOI: 10.48550/arXiv.1910.02490. URL: http://arxiv.org/abs/1910.02490 (visited on 09/29/2025).

[26] Wenxin Wu et al. “YOLO-SLAM: A semantic SLAM system towards dynamic environment with geometric constraint”. en. In: *Neural Computing and Applications* 34.8 (Apr. 2022), pp. 6011–6026. ISSN: 1433-3058. DOI: 10.1007/s00521-021-06764-3. URL: https://doi.org/10.1007/s00521-021-06764-3 (visited on 09/29/2025).

[27] Jiayuan Liu et al. “MAR-VO: A Match-and-Refine Framework for UAV’s Monocular Visual Odometry in Planetary Environments”. In: *IEEE Transactions on Geoscience and Remote Sensing* 63 (2025), pp. 1–14. ISSN: 1558-0644. DOI: 10.1109/TGRS.2025.3534581. URL: https://ieeexplore.ieee.org/abstract/document/10854502 (visited on 09/30/2025).

[28] Lukas Von Stumberg, Vladyslav Usenko, and Daniel Cremers. “Direct Sparse Visual-Inertial Odometry Using Dynamic Marginalization”. In: *2018 IEEE International Conference on Robotics and Automation (ICRA)*. ISSN: 2577-087X. May 2018, pp. 2510–2517. DOI: 10.1109/ICRA.2018.8462905. URL: https://ieeexplore.ieee.org/abstract/document/8462905 (visited on 09/25/2025).

[29] Michael Bloesch et al. “Robust visual inertial odometry using a direct EKF-based approach”. In: *2015 IEEE/RSJ International Conference on Intelligent Robots and Systems (IROS)*. Sept. 2015, pp. 298–304. DOI: 10.1109/IROS.2015.7353389. URL: https://ieeexplore.ieee.org/abstract/document/7353389 (visited on 09/25/2025).

[30] Carlos Campos et al. “ORB-SLAM3: An Accurate Open-Source Library for Visual, Visual–Inertial, and Multimap SLAM”. In: *IEEE Transactions on Robotics* 37.6 (Dec. 2021), pp. 1874–1890. ISSN: 1941-0468. DOI: 10.1109/TRO.2021.3075644. URL: https://ieeexplore.ieee.org/abstract/document/9440682 (visited on 09/25/2025).

[31] Andrew J. Davison et al. “MonoSLAM: Real-Time Single Camera SLAM”. In: *IEEE Transactions on Pattern Analysis and Machine Intelligence* 29.6 (June 2007), pp. 1052–1067. ISSN: 1939-3539. DOI: 10.1109/TPAMI.2007.1049. URL: https://ieeexplore.ieee.org/document/4160954 (visited on 09/27/2025).

[32] Georg Klein and David Murray. “Parallel Tracking and Mapping for Small AR Workspaces”. In: *2007 6th IEEE and ACM International Symposium on Mixed and Augmented Reality*. Nov. 2007, pp. 225–234. DOI: 10.1109/ISMAR.2007.4538852. URL: https://ieeexplore.ieee.org/abstract/document/4538852 (visited on 09/27/2025).

[33] Richard A. Newcombe, Steven J. Lovegrove, and Andrew J. Davison. “DTAM: Dense tracking and mapping in real-time”. In: *2011 International Conference on Computer Vision*. ISSN: 2380-7504. Nov. 2011, pp. 2320–2327. DOI: 10.1109/ICCV.2011.6126513. URL: https://ieeexplore.ieee.org/document/6126513 (visited on 09/27/2025).

[34] Richard A. Newcombe et al. “KinectFusion: Real-time dense surface mapping and tracking”. In: *2011 10th IEEE International Symposium on Mixed and Augmented Reality*. Oct. 2011, pp. 127–136. DOI: 10.1109/ISMAR.2011.6092378. URL: https://ieeexplore.ieee.org/abstract/document/6162880 (visited on 09/27/2025).

[35] Chenyang Shi et al. “A Review of Event-Based Indoor Positioning and Navigation.” In: *IPIN-WiP* (2022).

[36] Aditya NG et al. “Thermal Voyager: A Comparative Study of RGB and Thermal Cameras for Night-Time Autonomous Navigation”. In: *2024 IEEE International Conference on Robotics and Automation (ICRA)*. May 2024, pp. 14116–14122. DOI: 10.1109/ICRA57147.2024.10611311. URL: https://ieeexplore.ieee.org/document/10611311 (visited on 09/30/2025).

[37] Relja Arandjelovic et al. “NetVLAD: CNN Architecture for Weakly Supervised Place Recognition”. In: *2016 IEEE Conference on Computer Vision and Pattern Recognition (CVPR)*. ISSN: 1063-6919. June 2016, pp. 5297–5307. DOI: 10.1109/CVPR.2016.572. URL: https://ieeexplore.ieee.org/document/7780941 (visited on 09/30/2025).

[38] Antoni Rosinol, John J. Leonard, and Luca Carlone. “NeRF-SLAM: Real-Time Dense Monocular SLAM with Neural Radiance Fields”. In: *2023 IEEE/RSJ International Conference on Intelligent Robots and Systems (IROS)*. ISSN: 2153-0866. Oct. 2023, pp. 3437–3444. DOI: 10.1109/IROS55552.2023.10341922. URL: https://ieeexplore.ieee.org/abstract/document/10341922 (visited on 09/30/2025).

[39] Zihan Zhu et al. “NICE-SLAM: Neural Implicit Scalable Encoding for SLAM”. en. In: 2022, pp. 12786–12796. URL: https://openaccess.thecvf.com/content/CVPR2022/html/Zhu_NICE-SLAM_Neural_Implicit_Scalable_Encoding_for_SLAM_CVPR_2022_paper.html (visited on 09/30/2025).

[40] Zhen Hong et al. “SP-SLAM: Neural Real-Time Dense SLAM With Scene Priors”. In: *IEEE Transactions on Circuits and Systems for Video Technology* 35.6 (June 2025), pp. 5182–5194. ISSN: 1558-2205. DOI: 10.1109/TCSVT.2025.3526645. URL: https://ieeexplore.ieee.org/abstract/document/10830563 (visited on 09/30/2025).

[41] Eder A. Rodríguez-Martínez et al. “Vision-Based Navigation and Perception for Autonomous Robots: Sensors, SLAM, Control Strategies, and Cross-Domain Applications—A Review”. en. In: *Eng* 6.7 (July 2025). Publisher: Multidisciplinary Digital Publishing Institute, p. 153. ISSN: 2673-4117. DOI: 10.3390/eng6070153. URL: https://www.mdpi.com/2673-4117/6/7/153 (visited on 09/27/2025).

[42] Jonas Kühne et al. “Efficient and Accurate Downfacing Visual Inertial Odometry”. In: *IEEE Internet of Things Journal* (2025). arXiv:2509.10021 [cs], pp. 1–1. ISSN: 2327-4662, 2372-2541. DOI: 10.1109/JIOT.2025.3609011. URL: http://arxiv.org/abs/2509.10021 (visited on 09/24/2025).

[43] Yuhang Wang et al. “Lightweight visual localization algorithm for UAVs”. en. In: *Scientific Reports* 15.1 (Feb. 2025), p. 6069. ISSN: 2045-2322. DOI: 10.1038/s41598-025-88089-y. URL: https://www.nature.com/articles/s41598-025-88089-y (visited on 09/24/2025).

[44] Christian Kerl, Jürgen Sturm, and Daniel Cremers. “Dense visual SLAM for RGB-D cameras”. In: *2013 IEEE/RSJ International Conference on Intelligent Robots and Systems*. ISSN: 2153-0866. Nov. 2013, pp. 2100–2106. DOI: 10.1109/IROS.2013.6696650. URL: https://ieeexplore.ieee.org/abstract/document/6696650 (visited on 09/27/2025).

[45] Renato F. Salas-Moreno et al. “SLAM++: Simultaneous Localisation and Mapping at the Level of Objects”. In: *Proceedings of the IEEE Conference on Computer Vision and Pattern Recognition (CVPR)*. June 2013.

[46] Jakob Engel, Thomas Schöps, and Daniel Cremers. “LSD-SLAM: Large-Scale Direct Monocular SLAM”. en. In: *Computer Vision – ECCV 2014*. Ed. by David Fleet et al. Cham: Springer International Publishing, 2014, pp. 834–849. ISBN: 978-3-319-10605-2. DOI: 10.1007/978-3-319-10605-2_54.

[47] Felix Endres et al. “3-D Mapping With an RGB-D Camera”. In: *IEEE Transactions on Robotics* 30.1 (Feb. 2014), pp. 177–187. ISSN: 1941-0468. DOI: 10.1109/TRO.2013.2279412. URL: https://ieeexplore.ieee.org/document/6594910 (visited on 09/27/2025).

[48] Christian Forster, Matia Pizzoli, and Davide Scaramuzza. “SVO: Fast semi-direct monocular visual odometry”. In: *2014 IEEE International Conference on Robotics and Automation (ICRA)*. ISSN: 1050-4729. May 2014, pp. 15–22. DOI: 10.1109/ICRA.2014.6906584. URL: https://ieeexplore.ieee.org/document/6906584 (visited on 09/27/2025).

[49] Keisuke Tateno et al. *CNN-SLAM: Real-time dense monocular SLAM with learned depth prediction*. arXiv:1704.03489 [cs]. Apr. 2017. DOI: 10.48550/arXiv.1704.03489. URL: http://arxiv.org/abs/1704.03489 (visited on 09/27/2025).

[50] Raúl Mur-Artal and Juan D. Tardós. “ORB-SLAM2: An Open-Source SLAM System for Monocular, Stereo, and RGB-D Cameras”. In: *IEEE Transactions on Robotics* 33.5 (Oct. 2017), pp. 1255–1262. ISSN: 1941-0468. DOI: 10.1109/TRO.2017.2705103. URL: https://ieeexplore.ieee.org/document/7946260 (visited on 09/27/2025).

[51] Raúl Mur-Artal and Juan D. Tardós. “Visual-Inertial Monocular SLAM With Map Reuse”. In: *IEEE Robotics and Automation Letters* 2.2 (Apr. 2017), pp. 796–803. ISSN: 2377-3766. DOI: 10.1109/LRA.2017.2653359. URL: https://ieeexplore.ieee.org/document/7817784 (visited on 09/27/2025).

[52] Shujie Zhou et al. *LIR-LIVO: A Lightweight,Robust LiDAR/Vision/Inertial Odometry with Illumination-Resilient Deep Features*. arXiv:2502.08676 [cs]. Feb. 2025. DOI: 10.48550/arXiv.2502.08676. URL: http://arxiv.org/abs/2502.08676 (visited on 10/01/2025).

[53] Ryosuke Kataoka et al. “ICP-based SLAM Using LiDAR Intensity and Near-infrared Data”. In: *2021 IEEE/SICE International Symposium on System Integration (SII)*. ISSN: 2474-2325. Jan. 2021, pp. 100–104. DOI: 10.1109/IEEECONF49454.2021.9382647. URL: https://ieeexplore.ieee.org/document/9382647 (visited on 10/01/2025).

[54] Zheng Fan et al. “LiDAR, IMU, and camera fusion for simultaneous localization and mapping: a systematic review”. en. In: *Artificial Intelligence Review* 58.6 (Mar. 2025), p. 174. ISSN: 1573-7462. DOI: 10.1007/s10462-025-11187-w. URL: https://doi.org/10.1007/s10462-025-11187-w (visited on 10/01/2025).

[55] De Jong Yeong, Krishna Panduru, and Joseph Walsh. “Exploring the Unseen: A Survey of Multi-Sensor Fusion and the Role of Explainable AI (XAI) in Autonomous Vehicles”. en. In: *Sensors* 25.3 (Jan. 2025). Publisher: Multidisciplinary Digital Publishing Institute, p. 856. ISSN: 1424-8220. DOI: 10.3390/s25030856. URL: https://www.mdpi.com/1424-8220/25/3/856 (visited on 10/01/2025).

[56] Sidharth Jeyabal et al. “Hard-to-Detect Obstacle Mapping by Fusing LIDAR and Depth Camera”. In: *IEEE Sensors Journal* 24.15 (Aug. 2024), pp. 24690–24698. ISSN: 1558-1748. DOI: 10.1109/JSEN.2024.3409623. URL: https://ieeexplore.ieee.org/document/10552642 (visited on 10/01/2025).

[57] Yujeong Chae, Hyeonseong Kim, and Kuk-Jin Yoon. “Towards Robust 3D Object Detection with LiDAR and 4D Radar Fusion in Various Weather Conditions”. In: *2024 IEEE/CVF Conference on Computer Vision and Pattern Recognition (CVPR)*. ISSN: 2575-7075. June 2024, pp. 15162–15172. DOI: 10.1109/CVPR52733.2024.01436. URL: https://ieeexplore.ieee.org/document/10656703 (visited on 10/03/2025).

[58] Janis Tiemann, Andrew Ramsey, and Christian Wietfeld. “Enhanced UAV Indoor Navigation through SLAM-Augmented UWB Localization”. In: *2018 IEEE International Conference on Communications Workshops (ICC Workshops)*. ISSN: 2474-9133. May 2018, pp. 1–6. DOI: 10.1109/ICCW.2018.8403539. URL: https://ieeexplore.ieee.org/document/8403539/ (visited on 10/03/2025).

[59] H. A. G. C. Premachandra et al. “UWB Radar SLAM: An Anchorless Approach in Vision Denied Indoor Environments”. In: *IEEE Robotics and Automation Letters* 8.9 (Sept. 2023), pp. 5299–5306. ISSN: 2377-3766. DOI: 10.1109/LRA.2023.3293354. URL: https://ieeexplore.ieee.org/document/10175555/ (visited on 10/03/2025).

[60] Rogerio R Lima and Guilherme A S Pereira. “A multi-model framework for tether-based drone localization”. en. In: *J. Intell. Robot. Syst.* 108.2 (June 2023).

[61] L.A. Sandino et al. “Tether-guided landing of unmanned helicopters without GPS sensors”. In: *2014 IEEE International Conference on Robotics and Automation (ICRA)*. ISSN: 1050-4729. May 2014, pp. 3096–3101. DOI: 10.1109/ICRA.2014.6907304. URL: https://ieeexplore.ieee.org/document/6907304/ (visited on 10/14/2025).

[62] Marco M. Nicotra, Roberto Naldi, and Emanuele Garone. “Taut Cable Control of a Tethered UAV”. In: *IFAC Proceedings Volumes*. 19th IFAC World Congress 47.3 (Jan. 2014), pp. 3190–3195. ISSN: 1474-6670. DOI: 10.3182/20140824-6-ZA-1003.02581. URL: https://www.sciencedirect.com/science/article/pii/S1474667016420987 (visited on 10/15/2025).

[63] Francisco Alarcón et al. “A Precise and GNSS-Free Landing System on Moving Platforms for Rotary-Wing UAVs”. en. In: *Sensors* 19.4 (Jan. 2019). Publisher: Multidisciplinary Digital Publishing Institute, p. 886. ISSN: 1424-8220. DOI: 10.3390/s19040886. URL: https://www.mdpi.com/1424-8220/19/4/886 (visited on 10/14/2025).

[64] Amer Al-Radaideh and Liang Sun. “Self-Localization of Tethered Drones without a Cable Force Sensor in GPS-Denied Environments”. In: *Drones* 5.4 (2021). ISSN: 2504-446X.

[65] Leonhard Euler. *The rational mechanics of flexible or elastic bodies 1638-1788: introduction to Vol. X and XI*. Springer Science & Business Media, 1980.

[66] Seiga Kiribayashi, Kaede Yakushigawa, and Keiji Nagatani. “Position estimation of tethered micro unmanned aerial vehicle by observing the slack tether”. In: *2017 IEEE International Symposium on Safety, Security and Rescue Robotics (SSRR)*. ISSN: 2475-8426. Oct. 2017, pp. 159–165. DOI: 10.1109/SSRR.2017.8088157. URL: https://ieeexplore.ieee.org/document/8088157/ (visited on 10/14/2025).

[67] Xuesu Xiao et al. “Indoor UAV Localization Using a Tether”. In: *2018 IEEE International Symposium on Safety, Security, and Rescue Robotics (SSRR)*. 2018, pp. 1–6.

[68] Andrea Borgese et al. “Tether-Based Localization for Cooperative Ground and Aerial Vehicles”. In: *IEEE Robotics and Automation Letters* 7.3 (2022), pp. 8162–8169.

[69] E H Lockwood. *Book of Curves*. Cambridge, England: Cambridge University Press, Dec. 2007.

References

[1] Nicolas Mangold et al. “Perseverance rover reveals an ancient delta-lake system and flood deposits at Jezero crater, Mars”. In: *Science* 374.6568 (2021), pp. 711–717.

[2] J Balaram, MiMi Aung, and Matthew P Golombek. “The ingenuity helicopter on the perseverance rover”. In: *Space Science Reviews* 217.4 (2021), p. 56.

[3] D.C. Agle. *NASA Performs First Aircraft Accident Investigation on Another World*. 2024. URL: https://www.jpl.nasa.gov/news/nasa-performs-first-aircraft-accident-investigation-on-another-world/.

[4] S.O. Folorunsho and W.R. Norris. “Redefining aerial innovation: Autonomous tethered drones as a solution to battery life and data latency challenges”. In: (2024). eprint: 2403.07922 (cs.RO).